

Towards Real-World Test-Time Adaptation: Tri-net Self-Training with Balanced Normalization

Yongyi Su¹, Xun Xu^{2, 1*}, Kui Jia^{3*}

¹South China University of Technology

²Institute for Infocomm Research, A*STAR

³School of Data Science, The Chinese University of Hong Kong, Shenzhen
eesuyongyi@mail.scut.edu.cn, alex.xun.xu@gmail.com, kuijia@cuhk.edu.cn

Abstract

Test-Time Adaptation aims to adapt source domain model to testing data at inference stage with success demonstrated in adapting to unseen corruptions. However, these attempts may fail under more challenging real-world scenarios. Existing works mainly consider real-world test-time adaptation under non-i.i.d. data stream and continual domain shift. In this work, we first complement the existing real-world TTA protocol with a globally class imbalanced testing set. We demonstrate that combining all settings together poses new challenges to existing methods. We argue the failure of state-of-the-art methods is first caused by indiscriminately adapting normalization layers to imbalanced testing data. To remedy this shortcoming, we propose a balanced batchnorm layer to swap out the regular batchnorm at inference stage. The new batchnorm layer is capable of adapting without biasing towards majority classes. We are further inspired by the success of self-training (ST) in learning from unlabeled data and adapt ST for test-time adaptation. However, ST alone is prone to over adaption which is responsible for the poor performance under continual domain shift. Hence, we propose to improve self-training under continual domain shift by regularizing model updates with an anchored loss. The final TTA model, termed as TRIBE, is built upon a tri-net architecture with balanced batchnorm layers. We evaluate TRIBE on four datasets representing real-world TTA settings. TRIBE consistently achieves the state-of-the-art performance across multiple evaluation protocols. The code is available at <https://github.com/Gorilla-Lab-SCUT/TRIBE>.

Introduction

The recent success of deep neural networks relies on the assumption of generalizing pre-trained model to i.i.d. testing domain (Wang et al. 2022a). When deep learning models are to be deployed on real-world applications, robustness to out-of-distribution testing data, e.g. visual corruptions caused by lighting conditions, adverse weather, etc. becomes a major concern. Recent studies revealed such corruptions could severely deteriorate the generalization of model pre-trained on clean training samples (Sun et al. 2022; Hendrycks and Dietterich 2019; Sakaridis, Dai, and Van Gool 2018). Importantly, the corruption on testing data is often unknown and

sometimes unpredictable before deployment. Therefore, a new line of works emerge by adapting pre-trained models to testing data distribution at inference stage, a.k.a. test-time adaptation (TTA) (Sun et al. 2020; Wang et al. 2021; Su, Xu, and Jia 2022). The success of test-time adaptation is often achieved by distribution alignment (Su, Xu, and Jia 2022; Liu et al. 2021), self-supervised training (Chen et al. 2022) and self-training (Goyal et al. 2022), all demonstrating remarkable improvement of robustness on multiple types of visual corruptions in the testing data. Despite the unprecedented performance, existing TTA approaches are often developed under restrictive assumptions of testing data, e.g. stationary class distribution and static domain shift, and this gives rise to many attempts to explore TTA methods for real-world testing data (Wang et al. 2022b; Yuan, Xie, and Li 2023; Gong et al. 2022; Niu et al. 2023).

The recently explored real-world TTA, a.k.a. wild TTA (Niu et al. 2023) or Practical TTA (Yuan, Xie, and Li 2023), settings mainly consider the challenges brought by local class-imbalance (Niu et al. 2023; Yuan, Xie, and Li 2023; Gong et al. 2022) and continual domain shift (Wang et al. 2022b) which are expected to be encountered in real-world applications. Local class-imbalance is often observed when testing data are drawn in a non-i.i.d. manner (Gong et al. 2022). Direct adaptation indiscriminately results in biased distribution estimation and the recent works proposed exponential batchnorm update (Yuan, Xie, and Li 2023) or instance batchnorm update (Gong et al. 2022) to tackle this challenge. In this work, our aim is to address beyond the local class-imbalance challenge by taking into account the fact that the global distribution of testing data could be severely imbalanced and the class distribution may shift over time. We provide an illustration of the more challenging scenario in Fig. 1. This additional challenge renders existing TTA methods ineffective as the class prevalence on testing data is unknown before inference stage and the model could be biased towards majority classes through blind test-time adaptation. Through empirical observations, this issue becomes particularly acute for methods relying on estimating global statistics for updating normalization layers (Nado et al. 2020; Lee et al. 2013; Wang et al. 2021). It mainly owes to the fact that a single global distribution is estimated from the whole testing data on which samples are normalized. As such, the global distribution could easily bias towards majority classes,

*Correspondence to alex.xun.xu@gmail.com and kuijia@cuhk.edu.cn.

Copyright © 2024, Association for the Advancement of Artificial Intelligence (www.aaai.org). All rights reserved.

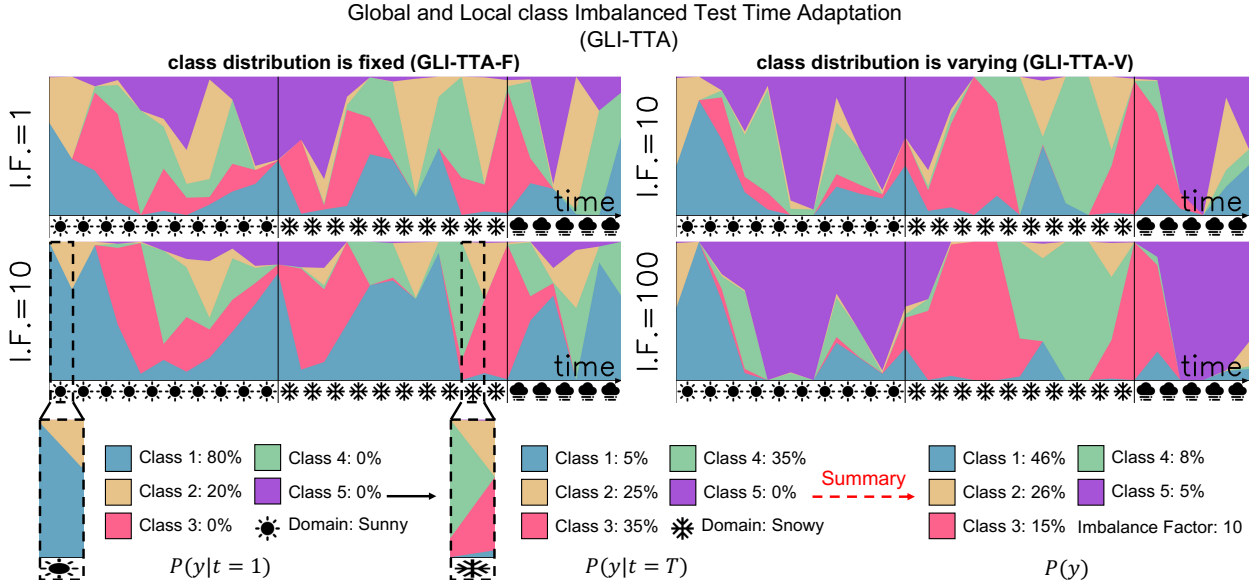


Figure 1: Illustration of two challenging real-world TTA scenarios. Different colors indicate the proportions of semantic classes, horizontal axis indicates testing data domain (e.g. different corruptions) may shift over time and different imbalance factor (I.F.) controls the degree of global imbalance. We expect the testing data stream to exhibit both local and global class imbalance, termed as “class distribution is fixed (GLI-TTA-F)” and this distribution may also evolve over time, termed as “class distribution is varying (GLI-TTA-V)”.

resulting in internal covariate shift (Ioffe and Szegedy 2015). To avoid biased batch normalization (BN), we propose a balanced batch normalization layer by modeling the distribution for each individual category and the global distribution is extracted from category-wise distributions. The balanced BN allows invariant estimation of distribution under both locally and globally class-imbalanced testing data.

Shift of domain over time occurs frequently in real-world testing data, e.g. a gradual change of lighting/weather conditions. It poses another challenge to existing TTA methods as the model could overly adapt to domain A and struggle with domain B when A shifts to B. To alleviate overly adapting to a certain domain, CoTTA (Wang et al. 2022b) randomly reverts model weights to pre-trained weights and EATA (Niu et al. 2022) regularizes the adapted model weights against source pre-trained weights to avoid overly shifting model weights. Nevertheless, these approaches still do not explicitly address the challenge of constant shifting domains in testing data. As self-training has been demonstrated to be effective for learning from unlabeled data (Sohn et al. 2020), we adopt a teacher-student framework for TTA. Nonetheless, direct self-training without regularization is prone to confirmation bias (Arazo et al. 2020) and could easily overly adapt pre-trained model to a certain domain, causing degenerate performance upon seeing new domains. To avoid this over adaptation, we further introduce an anchor network, of which the weights are copied from pre-trained model and batch-norm layers are dynamically updated by testing samples. The anchored loss, realised as mean square error (MSE), between teacher and anchor network is jointly optimised with self-training loss to strike a balance between adaptation to specific

domain and being versatile on ever changing domains. We brand this design as a tri-net architecture. We demonstrate that with the help of tri-net, TTA maintains a good performance within a wider range of learning rate. We refer to the final model as **TRI**-net self training with **Balance**d normalization (**TRIBE**) in recognition of the tri-net architecture with balanced normalization layer.

We summarize the contributions of this work as follows.

- We are motivated by the challenges in real-world test-time adaptation and propose to tackle a challenging TTA setting where testing data is both locally and globally class-imbalanced and testing domain may shift over time.
- A novel balanced batch normalization layer is introduced to fit to testing data distribution with both local and global class imbalance.
- We further introduce a tri-net framework to facilitate adaptation under continually shifting testing domain. We demonstrate this tri-net design improves robustness to the choice of learning rate.
- We evaluate the proposed method, TRIBE, on four test-time adaptation datasets under different real-world scenarios, demonstrating superior performance to all state-of-the-art methods.

Related Work

Unsupervised Domain Adaptation: Machine learning models often assume both training and testing data are drawn i.i.d. from the same distribution. When such assumption is violated, generalizing source model to testing distribution is

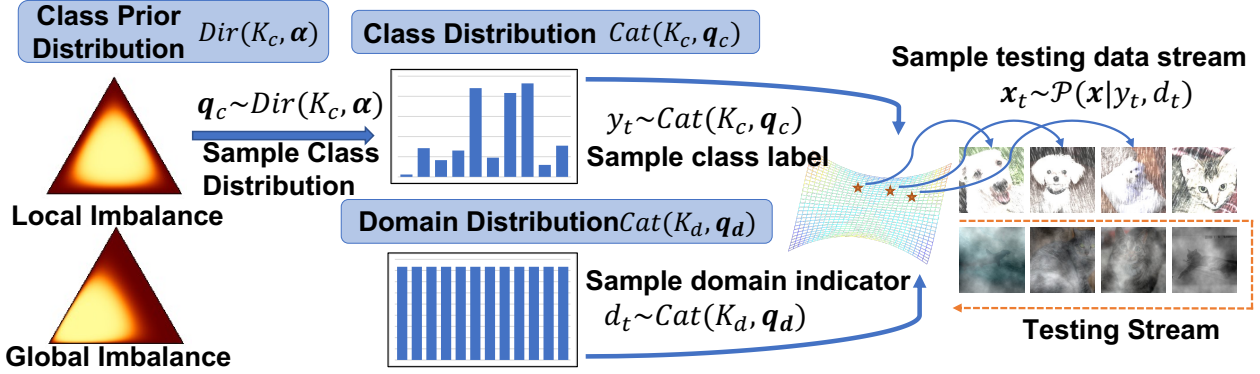


Figure 2: An illustration of the proposed real-world TTA simulation protocol with a hierarchical probabilistic model. A non-uniform α results in globally imbalanced testing data distribution.

hampered by the domain shift, leading to degraded performance (Wang and Deng 2018). Unsupervised domain adaptation (UDA) improves model generalization by exploiting both labeled source domain data and unlabeled target domain data (Ganin and Lempitsky 2015; Tzeng et al. 2014; Long et al. 2015). Common approaches towards UDA includes distribution alignment (Gretton et al. 2012; Sun and Saenko 2016; Zellinger et al. 2016), adversarial learning (Hoffman et al. 2018), target clustering (Tang, Chen, and Jia 2020) and self-training (Liu, Wang, and Long 2021). Nevertheless, UDA is only effective when source and target domain data are simultaneously accessible. More importantly, in real-world applications the distribution in target domain is often predictable until inference stage which has motivated research into test-time adaptation.

Test-Time Adaptation: Adapting pre-trained model to target domain distribution at test-time improves model generalization to unseen distribution shift. Widely adopted test-time adaptation (TTA) protocol simultaneously evaluate on a stream of testing data and update model weights (Sun et al. 2020; Wang et al. 2021; Iwasawa and Matsuo 2021; Su, Xu, and Jia 2022; Gandselman et al. 2022; Goyal et al. 2022; Chen et al. 2022). The state-of-the-art approaches towards TTA adopt self-training (Wang et al. 2021; Su et al. 2023; Gandselman et al. 2022), distribution alignment (Sun et al. 2020; Su, Xu, and Jia 2022) and self-supervised learning (Liu et al. 2021; Chen et al. 2022). With the above techniques, generalization performance on testing data with corruptions has been substantially improved. Nonetheless, most of these are optimized towards the vanilla TTA protocol, thus these methods may not maintain the superior performance under more realistic TTA scenarios.

Real-World Test-Time Adaptation: Deploying TTA methods in real-world application requires tackling commonly encountered challenges. Recent works summarized multiple challenges that could appear in real-world test-time adaptation, including updating with small batchsize (Niu et al. 2023), non-i.i.d. or temporally correlated testing data (Gong et al. 2022; Wang et al. 2022b; Yuan, Xie, and Li 2023; Boudiaf et al. 2022) and continually adapting to shifting do-

mains (Wang et al. 2022b; Yuan, Xie, and Li 2023; Brahma and Rai 2023). Empirical observations demonstrate that these real-world challenges could pose great challenges to existing TTA methods. Despite the recent efforts in developing TTA robust to non-i.i.d. testing data, we argue that a systematic investigation into more diverse real-world challenges, including global class-imbalance, is missing. This work propose a principled way to simulate these challenges and develop a self-training based method with balanced batchnorm to achieve the state-of-the-art performance.

Methodology

Real-World TTA Protocol

We denote a stream of testing data as $\mathbf{x}_0, \mathbf{x}_1, \dots, \mathbf{x}_T$ where each \mathbf{x}_t is assumed to be drawn from a distribution $\mathcal{P}(\mathbf{x}|d_t, y_t)$ conditioned on two time-varying variables, namely the testing domain indicator $d_t \in \{1, \dots, K_d\}$ and the class label $y_t \in \{1, \dots, K_c\}$, where K_d and K_c refer to the number of domains (e.g. type of corruptions) and number of semantic classes. In the real-world TTA protocol, both the testing domain indicator and class label distribution could be subject to constant shift, in particular, we assume the domain indicator to exhibit a gradual and slowly shift over time. This is manifested by many real-world applications, e.g. the lighting and weather conditions often changes slowly. We further point out that testing samples are often class imbalanced both locally within a short period of time and globally over the whole testing data stream. Therefore, we model the testing data stream as sampling from a hierarchical probabilistic model. Specifically, we denote a prior $\alpha \in \mathbb{R}^{K_c}$ parameterizing a Dirichlet distribution $\mathbf{q}_c \sim Dir(K_c, \alpha)$. Within a stationary local time window, e.g. a minibatch of testing samples, the labels of testing samples are drawn from a categorical distribution $y \sim Cat(K_c, \mathbf{q}_c)$ where \mathbf{q}_c is drawn from the conjugate prior distribution $Dir(K_c, \alpha)$. The corrupted testing sample is then assumed to be finally sampled from a complex distribution conditioned on the domain indicator d_t and class label y_t , written as $\mathbf{x} \sim \mathcal{P}(\mathbf{x}|d_t, y_t)$. The domain indicator can be modeled as another categorical distribution parameterized by a fixed probability $d_t \sim Cat(K_d, \mathbf{q}_d)$. A

hierarchical probabilistic model simulating the real-world TTA protocol is presented in Fig. 2. We notice the probabilistic model can instantiate multiple existing TTA protocols. For instance, when testing data are locally class imbalanced, as specified by (Yuan, Xie, and Li 2023; Gong et al. 2022), a uniform proportion parameter $\alpha = \sigma \mathbf{1}$ is chosen with a scale parameter σ controlling the degree of local imbalancedness and \mathbf{q}_c is re-sampled every mini-batch. We can easily simulate global class-imbalance by specifying a non-uniform α . We defer a more detailed discussion of simulating real-world TTA protocols with the hierarchical probabilistic model to the supplementary.

Balanced Batch Normalization

Batch normalization (BN) (Ioffe and Szegedy 2015) plays a critical role in enabling more stable model training, reducing sensitivity to hyper-parameters and initialization. When testing data features a distribution shift from the source training data, the regular practice of freezing BN statistics for inference fails to maintain the generalization (Yuan, Xie, and Li 2023; Nado et al. 2020; Gong et al. 2022; Lim et al. 2023; Niu et al. 2023). Hence, adapting BN statistics to testing data distribution becomes a viable solution to TTA (Nado et al. 2020). To adapt model subject to locally imbalanced testing data, the robust batch normalization (Yuan, Xie, and Li 2023) updates BN’s mean and variance in a moving average manner on testing data. The robust BN smooths out the bias estimated within each minibatch and achieves competitive performance under non-i.i.d. testing data stream.

Despite being successful in non-i.i.d. testing data stream, a naive moving average update policy struggles in adapting to globally imbalanced testing domain. For example, evidenced in the empirical evaluation in Tab. 1, the performance of RoTTA (Yuan, Xie, and Li 2023) degenerates substantially under more severely global imbalanced testing data. We ascribe the poor performance to the fact that a single BN will bias towards majority classes and normalizing samples from the minority classes with biased statistics will result in severe covariate shift within internal representations. This will eventually cause mis-classifying the minority classes and lower the macro average accuracy. To remedy the bias in adapting BN statistics, we propose a Balanced Batchnorm layer which maintains K_c pairs of statistics separately for each semantic class, denoted as $\{\mu_k\}_{k=1 \dots K_c}$, $\{\sigma_k\}_{k=1 \dots K_c}$. To update category-wise statistics, we apply an efficient iterative updating approach with the help of pseudo labels predictions as follows,

$$\begin{aligned} \mu_k^t &= \mu_k^{t-1} + \delta_k, \\ \sigma_k^{2t} &= \sigma_k^{2t-1} - \delta_k^2 + \eta \sum_{b=1}^B \mathbb{1}(\hat{y}_b = k) \frac{1}{HW} \sum_{h=1}^H \sum_{w=1}^W [(F_{bhw} - \mu_k^{t-1})^2 - \sigma_k^{2t-1}] \\ \text{s.t. } \delta_k &= \eta \sum_{b=1}^B \mathbb{1}(\hat{y}_b = k) \frac{1}{HW} \sum_{h=1}^H \sum_{w=1}^W (F_{bhw} - \mu_k^{t-1}), \end{aligned} \quad (1)$$

where $\mathbf{F} \in \mathbb{R}^{B \times C \times H \times W}$ denotes the input for Balanced BN layer and \hat{y}_b is the pseudo label predicted by the adapted model in the inference step. With the above design BN statistics for each individual class is separately updated and the

global BN statistics are derived from all category-wise statistics as in Eq. 2.

$$\mu_g = \frac{1}{K_c} \sum_{k=1}^{K_c} \mu_k^t, \quad \sigma_g^2 = \frac{1}{K_c} \sum_{k=1}^{K_c} [\sigma_k^{2t} + (\mu_g - \mu_k^t)^2]. \quad (2)$$

Nevertheless, we found when the number of categories is large or the pseudo labels are highly untrustworthy, e.g. the baseline accuracy on ImageNet-C is very low, the above updating strategy might be less effective due to its reliance on the pseudo labels. Therefore, we combine the class-agnostic updating strategy (Robust BN) and the category-wise updating strategy with a balancing parameter γ as below.

$$\mu_k^t = \mu_k^{t-1} + (1 - \gamma) \delta_k + \gamma \frac{1}{K_c} \sum_{k'=1}^{K_c} \delta_{k'}, \quad (3)$$

$$\begin{aligned} \sigma_k^{2t} &= \sigma_k^{2t-1} + \\ (1 - \gamma) &\left\{ -\delta_k^2 + \eta \sum_{b=1}^B \mathbb{1}(\hat{y}_b = k) \frac{1}{HW} \sum_{h=1}^H \sum_{w=1}^W [(F_{bhw} - \mu_k^{t-1})^2 - \sigma_k^{2t-1}] \right\} + \\ \gamma \cdot \frac{1}{K_c} \sum_{k'=1}^{K_c} &\left\{ -\delta_{k'}^2 + \eta \sum_{b=1}^B \mathbb{1}(\hat{y}_b = k') \frac{1}{HW} \sum_{h=1}^H \sum_{w=1}^W [(F_{bhw} - \mu_{k'}^{t-1})^2 - \sigma_{k'}^{2t-1}] \right\}. \end{aligned} \quad (4)$$

Specifically, when $\gamma = 0$ the updating strategy is the pure class-wise updating strategy and when $\gamma = 1$ the updating strategy degrades to the rule in Robust BN. In all experiments of this paper, we leverage $\gamma = 0.0$ in CIFAR10-C, $\gamma = 0.1$ in CIFAR100-C due to the large number of class and $\gamma = 0.5$ in ImageNet-C due to the highly untrustworthy pseudo labels. The instance-level momentum coefficient η in Balanced BN is set to $0.0005 \times K_c$.

Tri-Net Self-Training

Self-Training (ST) has demonstrated tremendous effectiveness in multiple tasks (Sohn et al. 2020; Kumar, Ma, and Liang 2020). ST updates the model through constraining the prediction consistency between original samples and corresponding augmented samples. In this work, we adopt an approach similar to semi-supervised learning (Sohn et al. 2020) to fine-tune the model to adapt the testing data. In specific, as illustrated in Fig. 3, we introduce teacher $f_t(\mathbf{x}; \Theta)$ and student $f_s(\mathbf{x}; \Theta)$ networks where the BN layers are independently updated while other weights are shared. The pseudo labels for testing sample are predicted by the teacher network and only the confident pseudo labels are employed for training the student network. Specifically, we denote the probabilistic posterior as $\mathbf{p} = h(f(\mathbf{x}))$ and define the self-training loss in Eq. 5, where $\mathbf{p}^s = h(f_s(\mathcal{A}(\mathbf{x}); \Theta))$, $\mathbf{p}^t = h(f_t(\mathbf{x}; \Theta))$, $\hat{\mathbf{p}}^t$ refers to the one-hot pseudo label of \mathbf{p}^t , \mathcal{A} refers to a strong data augmentation operation, \mathcal{H} refers to entropy and cross-entropy losses and H_0 defines a thresholding hyper-parameter.

$$\mathcal{L}_{st} = \frac{\sum_{b=1}^B \mathbb{1}(\mathcal{H}(\mathbf{p}_b^t) < H_0 \cdot \log K_c) \cdot \mathcal{H}(\hat{\mathbf{p}}_b^t, \mathbf{p}_b^s)}{\sum_{b=1}^B \mathbb{1}(\mathcal{H}(\mathbf{p}_b^t) < H_0 \cdot \log K_c)} \quad (5)$$

A recent study revealed that self-training is effective for TTA (Su et al. 2023), however without additional regularizations self-training is easily subject to confirmation bias (Arazo et al. 2020). This issue would only exacerbate

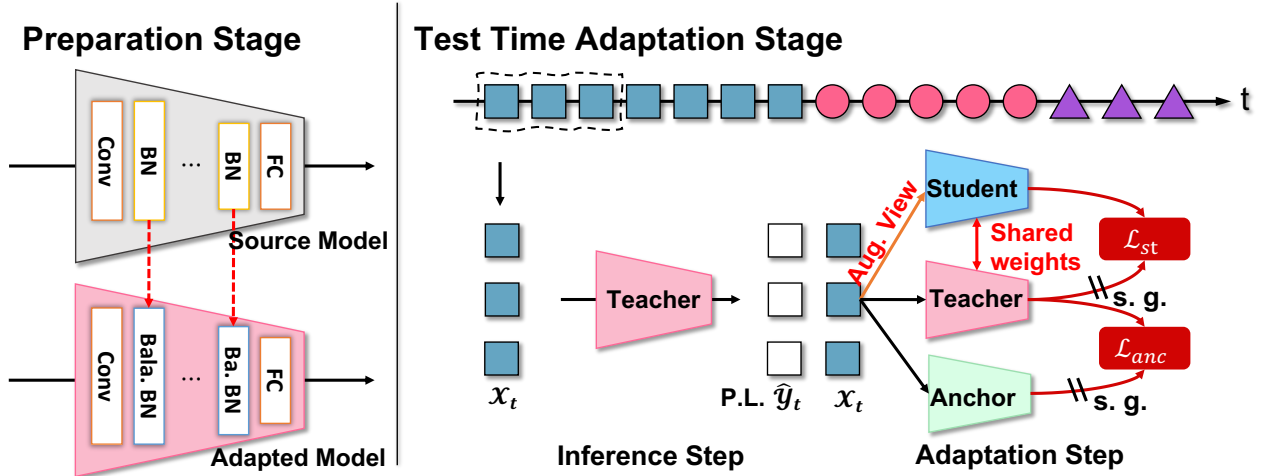


Figure 3: Illustration of the proposed method. We replace the Batchnorm layer of the source model with our proposed Balanced Batchnorm for imbalanced testing set. During test time adaptation, we optimize the combination of self-training loss \mathcal{L}_{st} and anchor loss \mathcal{L}_{anc} .

when test data distribution is highly imbalanced, thus leading to over adapting or collapsed predictions. To avoid over adapting model to a certain test domain, we further propose to incorporate an additional network branch as anchor for regularization.

Anchor Network: We use a frozen source domain network as the anchor network to regularize self-training. In particular, we copy the source model weights, freeze all weights and swap regular BN layers with the proposed Balanced BN layers. To regularize self-training, we design an anchored loss as the mean square error between the posterior predictions of teacher and anchor networks as in Eq. 6. As three network branches are jointly utilized, it gives rise to the term of tri-net self-training.

$$\mathcal{L}_{anc} = \frac{\sum_{b=1}^B \mathbb{1}(\mathcal{H}(\mathbf{p}_b^t) < H_0 \cdot \log K_c) \|\mathbf{p}_b^t - \mathbf{p}_b^a\|_2^2}{K_c \sum_{b=1}^B \mathbb{1}(\mathcal{H}(\mathbf{p}_b^t) < H_0 \cdot \log K_c)} \quad (6)$$

We finally simultaneously optimize the self-training and anchored losses $\mathcal{L} = \mathcal{L}_{st} + \lambda_{anc} \mathcal{L}_{anc}$ w.r.t. the affine parameters of the Balanced BN layers for efficient test-time adaptation.

Experiment

Experiment Settings

Datasets: We evaluate on four test-time adaptation datasets, including **CIFAR10-C** (Hendrycks and Dietterich 2019), **CIFAR100-C** (Hendrycks and Dietterich 2019), **ImageNet-C** (Hendrycks and Dietterich 2019) and **MNIST-C** (Mu and Gilmer 2019). Each of these benchmarks includes 15 types of corruptions with 5 different levels of severity. CIFAR10/100-C both have 10,000 testing samples evenly divided into 10/100 classes for each type of corruptions. ImageNet-C has 5,000 testing samples for each corruption unevenly di-

vided into 1,000 classes ¹. We evaluate all methods under the largest corruption severity level 5 and report the classification error rate (%) throughout the experiment section. We include the detailed results of **MNIST-C** (Mu and Gilmer 2019) in the supplementary.

Hyper-parameters: For CIFAR10-C and CIFAR100-C experiments, we follow the official implementations from previous TTA works (Wang et al. 2021, 2022b; Yuan, Xie, and Li 2023) and respectively adopt a standard pre-trained WideResNet-28 (Zagoruyko and Komodakis 2016) and ResNeXt-29 (Xie et al. 2017) models from Robust-Bench (Croce et al. 2021) benchmark, for the fair comparison. For ImageNet-C experiments, the standard pre-trained ResNet-50 (He et al. 2016) model in torchvision is adopted. For most competing methods and our TRIBE, we leverage the Adam (Kingma and Ba 2014) optimizer with the learning rate 1e-3 in CIFAR10/100-C and ImageNet-C experiments. As an exception, for Note (Gong et al. 2022) and TTAC (Su, Xu, and Jia 2022) we use the learning rate released in their official implementations. We use a batchsize of 64 for CIFAR10/100-C and 48 for ImageNet-C. Other hyper-parameters of our proposed model are listed as follow: $\lambda_{anc} = 0.5$, $\eta = 0.0005 \times K_c$ in all datasets, in CIFAR10-C $H_0 = 0.05$, $\gamma = 0$, in CIFAR100-C $H_0 = 0.2$, $\gamma = 0.1$ and in ImageNet-C $H_0 = 0.4$, $\gamma = 0.5$. Adequate hyper-parameter analysis, provided in the supplementary, demonstrate that the hyper-parameters used into TRIBE are not sensitive. The data augmentations used in TRIBE are described in the supplementary. All of our experiments can be performed on a single NVIDIA GeForce RTX 3090 card.

TTA Evaluation Protocol: We evaluate under two real-world TTA protocols, namely the **GLI-TTA-F** and **GLI-TTA-V**. For both protocols, we create a global class imbalanced testing set following the long-tail dataset creation protocol (Cui

¹ImageNet-C is only evaluated in a subset with 5,000 testing samples on RobustBench: <https://github.com/RobustBench/robustbench>

Method	Fixed Global Class Distribution (GLI-TTA-F)			
	I.F. = 1	I.F. = 10	I.F. = 100	I.F. = 200
TEST	43.50 / 43.50	42.64 / 43.79	41.71 / 43.63	41.69 / 43.47
BN	75.20 / 75.20	70.77 / 66.77	70.00 / 50.72	70.13 / 47.34
PL	82.90 / 82.90	72.43 / 70.59	70.09 / 55.29	70.38 / 49.86
TENT	86.00 / 86.00	78.15 / 74.90	71.10 / 58.59	69.15 / 53.37
LAME	39.50 / 39.50	38.45 / 40.07	37.48 / 41.80	37.52 / 42.59
COTTA	83.20 / 83.20	73.64 / 71.48	71.32 / 56.44	70.78 / 49.98
NOTE	31.10 / 31.10	36.79 / 30.22	42.59 / 30.75	45.45 / 31.17
TTAC	23.01 / 23.01	31.20 / 29.11	43.40 / 37.37	46.27 / 38.75
PETAL	81.05 / 81.05	73.97 / 71.64	71.14 / 56.11	71.05 / 50.57
RoTTA	25.20 / 25.20	27.41 / 26.31	30.50 / 29.08	32.45 / 30.04
TRIBE	16.14 / 16.14	20.98 / 22.49	19.53 / 24.66	19.16 / 24.00

Method	Time-Varying Global Class Distribution (GLI-TTA-V)			
	I.F. = 1	I.F. = 10	I.F. = 100	I.F. = 200
TEST	43.50 / 43.50	41.95 / 43.65	40.74 / 43.83	40.53 / 43.77
BN	75.20 / 75.20	71.36 / 67.70	70.35 / 53.07	70.88 / 50.67
PL	82.90 / 82.90	74.74 / 72.12	73.03 / 57.53	72.49 / 54.20
TENT	86.00 / 86.00	77.69 / 74.23	72.99 / 58.65	73.45 / 54.96
LAME	39.50 / 39.50	38.02 / 40.15	36.51 / 42.16	36.24 / 42.16
COTTA	83.20 / 83.20	75.29 / 71.87	73.83 / 56.80	74.97 / 56.47
NOTE	31.10 / 31.10	29.52 / 29.23	30.02 / 29.88	29.71 / 30.28
TTAC	23.01 / 23.01	32.25 / 32.12	36.84 / 37.13	37.96 / 38.07
PETAL	81.05 / 81.05	75.19 / 71.65	72.71 / 55.73	73.76 / 53.51
RoTTA	25.20 / 25.20	27.61 / 26.35	32.16 / 29.32	33.34 / 31.35
TRIBE	16.14 / 16.14	20.92 / 22.40	22.44 / 25.50	23.10 / 27.03

Table 1: Average classification error on CIFAR10-C while continually adapting to different corruptions at the highest severity 5 with globally and locally class-imbalanced test stream. *I.F.* is the Imbalance Factor of Global Class Imbalance. Instance-wise average error rate *a%* and category-wise average error rate *b%* are separated by (a / b).

et al. 2019), we choose three imbalance factor *I.F.* as 1, 10, 100 and 200 for evaluation where GLI-TTA degrades into PTTA setting (Yuan, Xie, and Li 2023) with *I.F. = 1*. A default scale parameter $\sigma = 0.1$ is chosen to control local class imbalance. To simulate continually shifting domains, we sample without replacement the domain indicator after all testing samples are predicted. For better reproducibility we provide the sequence of domains in the supplementary. Under the GLI-TTA-F setting, we fix the proportion parameter α throughout the experiment. Under the GLI-TTA-V setting, we randomly permute class indices after adaptation to each domain (type of corruption) to simulate time-varying class distribution.

Competing Methods: We benchmark against the following TTA methods (Nado et al. 2020; Lee et al. 2013; Wang et al. 2021; Boudiaf et al. 2022; Gong et al. 2022; Su, Xu, and Jia 2022; Yuan, Xie, and Li 2023; Niu et al. 2022). Direct testing (**TEST**) performs inference on test streaming data without adaptation. Prediction-time batch normalization (**BN**) (Nado et al. 2020) replaces the running statistics with the batch statistics on each testing minibatch for normalization. Pseudo Label (**PL**) (Lee et al. 2013) updates the parameters of all normalization layers by minimizing the cross-entropy loss with predicted pseudo labels. Test-time entropy minimization (**TENT**) (Wang et al. 2021) updates the affine parameters of all batchnorm layers by minimizing the entropy of predictions. Laplacian adjusted maximum-likelihood estimation

Method	Fixed Global Class Distribution (GLI-TTA-F)			
	I.F. = 1	I.F. = 10	I.F. = 100	I.F. = 200
TEST	46.40 / 46.40	46.96 / 46.52	47.53 / 45.91	47.59 / 39.94
BN	52.90 / 52.90	46.05 / 42.29	47.01 / 40.01	47.38 / 35.26
PL	88.90 / 88.90	68.51 / 69.71	53.46 / 57.26	49.41 / 49.26
TENT	92.80 / 92.80	76.88 / 79.08	56.72 / 65.96	50.45 / 58.45
LAME	40.50 / 40.50	43.66 / 44.88	44.15 / 46.64	43.81 / 40.33
COTTA	52.20 / 52.20	44.48 / 40.93	45.46 / 38.77	45.67 / 33.72
NOTE	73.80 / 73.80	57.71 / 58.86	54.44 / 57.10	53.74 / 52.48
TTAC	34.10 / 34.10	40.48 / 38.28	47.84 / 41.47	49.78 / 38.00
PETAL	55.03 / 55.03	45.14 / 41.91	44.63 / 38.52	44.75 / 33.81
RoTTA	35.00 / 35.00	40.00 / 39.03	45.68 / 42.04	46.78 / 37.93
TRIBE	33.26 / 33.26	33.10 / 34.31	32.31 / 34.98	32.29 / 31.54

Method	Time-Varying Global Class Distribution (GLI-TTA-V)			
	I.F. = 1	I.F. = 10	I.F. = 100	I.F. = 200
TEST	46.40 / 46.40	45.85 / 46.65	45.34 / 46.94	45.16 / 40.61
BN	52.90 / 52.90	45.10 / 42.47	45.15 / 38.80	45.37 / 33.45
PL	88.90 / 88.90	68.16 / 66.62	52.83 / 48.39	53.68 / 44.28
TENT	92.80 / 92.80	77.11 / 76.51	65.42 / 63.48	62.45 / 53.57
LAME	40.50 / 40.50	42.82 / 45.35	42.47 / 47.82	42.23 / 41.45
COTTA	52.20 / 52.20	43.74 / 41.03	43.83 / 37.93	43.96 / 32.69
NOTE	73.80 / 73.80	58.07 / 58.46	55.16 / 55.95	54.43 / 48.65
TTAC	34.10 / 34.10	38.56 / 38.68	42.07 / 41.05	42.87 / 35.80
PETAL	55.03 / 55.03	44.36 / 41.54	44.11 / 38.33	44.43 / 32.84
RoTTA	35.00 / 35.00	39.56 / 39.77	42.20 / 39.93	43.57 / 35.82
TRIBE	33.26 / 33.26	33.52 / 34.49	33.76 / 34.63	34.29 / 30.22

Table 2: Average classification error on CIFAR100-C while continually adapting to different corruptions at the highest severity 5 with globally and locally class-imbalanced test stream.

(**LAME**) (Boudiaf et al. 2022) adjusts the predictions of the model through maximizing the likelihood estimation without updating any parameters. Continual test-time adaptation (**COTTA**) (Wang et al. 2022b) performs mean-teacher architecture, and randomly selects and restores the parameters of the model to source model. **PETAL** (Brahma and Rai 2023) leverages fisher information to instruct the parameter restoration. Non-i.i.d. test-time adaptation (**NOTE**) (Gong et al. 2022) optionally updates the batchnorm statistics when the distance between the instance statistics of the test sample and the source model’s statistics is less than a threshold. Test-time anchored clustering (**TTAC**) (Su, Xu, and Jia 2022) minimizes the KL-Divergence between the source and target domain distributions. Robust test-time adaptation (**RoTTA**) (Yuan, Xie, and Li 2023) replaces the batchnorm layers with Robust Batch Normalization for better estimation of target domain batchnorm statistics. Finally, we evaluate our **TRIBE** with tri-net self-training and Balanced Batchnorm layers.

Real-World Test Time Adaptation Results

Under the proposed real-world test-time adaptation protocol, the classification errors averaged over continuously adapting to all 15 types of corruptions under different degrees of global imbalance are calculated. We report the results in Tab. 1 for CIFAR10-C and Tab. 2 for CIFAR100-C. We make the following observations from the results. i) Direct testing without any adaptation is even stronger than many TTA methods. For example, only LAME, TTAC, RoTTA and our TRIBE

Time	t																Avg.
Method		motion	snow	fog	shot	defocus	contrast	zoom	brightness	frost	elastic	glass	gaussian	pixelate	jpeg	impulse	
TEST		85.15	83.45	75.88	97.09	81.68	94.52	77.93	41.23	77.07	82.48	89.73	97.81	79.31	68.50	98.17	82.00
BN		73.64	66.07	52.81	84.49	85.05	82.66	61.96	36.04	68.60	56.44	84.85	85.31	52.29	60.77	85.05	69.07
PL		66.55	60.43	49.46	76.57	79.23	81.04	65.35	51.48	75.62	69.74	89.04	92.36	86.84	92.09	97.83	75.58
TENT		64.37	59.73	51.20	77.47	81.70	88.72	82.38	76.91	93.64	95.43	98.80	98.98	98.39	98.90	99.40	84.40
LAME		85.93	84.57	77.29	97.47	81.92	94.72	78.41	41.49	77.67	84.07	90.25	98.21	79.61	68.64	98.76	82.60
EATA		73.15	65.41	52.51	84.27	85.09	82.85	61.52	35.15	68.26	56.30	84.43	84.95	51.63	60.85	85.05	68.76
NOTE		82.97	78.29	73.43	93.92	96.35	89.73	93.18	84.57	92.82	94.54	98.50	98.88	98.17	97.55	98.78	91.44
ROTTA		74.86	70.02	55.26	85.55	85.37	78.61	61.00	34.31	64.65	52.83	76.16	85.43	48.70	52.41	78.37	66.90
TRIBE		69.52	59.55	48.35	79.27	78.47	75.54	56.62	35.19	60.39	49.26	74.54	74.10	50.08	51.24	72.59	62.32

Table 3: Average classification error on ImageNet-C while continually adapting to different corruptions at the highest severity 5 with non-i.i.d. testing data stream.

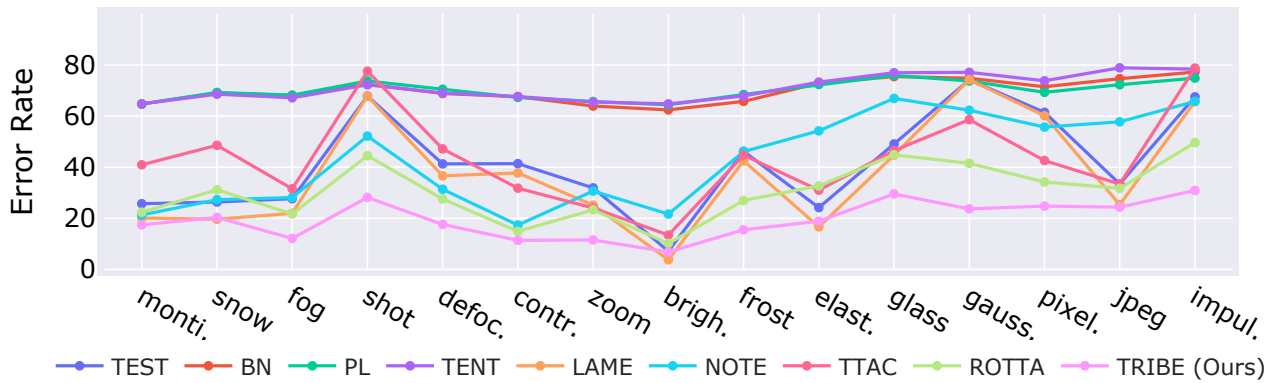


Figure 4: Performances on each individual domain (corruption) under GLI-TTA-F (I.F.=100) protocols on CIFAR10-C dataset.

could consistently outperform direct testing (TEST) on both CIFAR10-C and CIFAR100-C datasets, suggesting the necessity to develop robust TTA approaches. ii) Global class imbalance poses a great challenge to existing robust TTA methods. For example, the previous state-of-the-art, Rotta achieves 25.2% and 35.0% on CIFAR10-C and CIFAR100-C respectively, while the error rose to 30.04% and 37.93% under severely global imbalanced testing set ($I.F. = 200$). The same observation applies to other competing methods. In comparison, TRIBE is able to maintain relatively better performance under more severe global imbalanced testing set. iii) We further notice that TRIBE consistently outperform all competing methods in absolute accuracy. Importantly, under balanced global distribution ($I.F. = 1$), TRIBE outperforms the best performing model, TTAC, by 7% on CIFAR10-C. The margin is maintained under more imbalanced testing set ($I.F. = 200$). iv) TRIBE maintains a more consistent performance from $I.F. = 10$ to $I.F. = 200$ on both CIFAR10-C and CIFAR100-C, while other competing methods degenerate substantially. This is attributed to the introduction of Balanced BN layer better accounting for severe class imbalance and anchored loss avoiding over adaptation across the different domains.

We further evaluate TTA performance on ImageNet-C dataset of which the testing set is naturally class imbalanced. Therefore, we only simulate local class imbalance for the

testing data stream and allow α equal to the marginalized class distribution. We present both averaged and domain specific classification error in Tab. 3. We make similar observations with results on CIFAR10/100-C. Some competitive TTA methods perform exceptionally worse than direct testing while TRIBE again outperforms all competing methods both in terms of averaged error rate and winning on 11/15 corruption types.

Results on Individual Corruption: We adapt the model continually to constant shifting domains (corruption types). We report the average classification error for each individual type of corruptions in Fig. 4. We conclude from the plots that i) BN, PL and TENT normalize the features using the statistics calculated within current mini-batch, thus they all perform much worse than methods considering robust batchnorm e.g. NOTE, Rotta and TRIBE. ii) There is a strong correlation of performance across different methods suggesting certain corruptions, e.g. “shot”, “gaussian noise” and “impulse noise”, are inherently more difficult. Nevertheless, TRIBE always outperforms competing methods on these challenging corruptions. iii) Some competing methods achieve close to TRIBE accuracy on easier corruptions, but they often perform much worse on the upcoming corruptions. Overall, TRIBE exhibits much lower variance across all domains when continually adapted. This suggests the anchored loss potentially helps TRIBE to avoid over adapting to easier domains.

Method	EMA Model	BatchNorm	Self-Training	Anchored Loss	CIFAR10-C	CIFAR100-C	Avg.
TEST ROTTA	–	BN	–	–	41.71 / 43.63	47.53 / 45.91	44.62 / 44.77
	✓	Robust BN	✓	–	30.50 / 29.08	45.68 / 42.04	38.09 / 35.56
	–	Robust BN	–	–	43.48 / 32.29	40.45 / 36.94	41.97 / 34.62
	–	Balanced BN	–	–	29.00 / 26.38	39.55 / 36.59	34.28 / 31.49
	–	BN	✓	–	37.67 / 38.94	37.12 / 44.77	37.40 / 41.86
	–	Balanced BN	✓	–	36.58 / 65.88	37.21 / 44.83	36.90 / 55.36
	–	BN	✓	✓	36.76 / 29.19	36.16 / 36.26	36.46 / 32.73
MT*	✓	Balanced BN	✓	–	23.76 / 25.18	36.01 / 35.72	29.89 / 30.45
TRIBE	–	Balanced BN	✓	✓	19.53 / 24.66	32.31 / 34.98	25.92 / 29.82

Table 4: Ablation study on CIFAR10/100-C under GLI-TTA-F (*I.F.* = 100) protocol. We report classification error as evaluation metric. MT* indicates Mean Teacher is adapted to TTA task by removing the labeled loss term.

Method	Imbalance Factor			
	1	10	100	200
TEST	43.51	42.65	41.71	41.69
IABN (NIPS22)	27.29	31.74	38.19	40.03
Robust BN (5e-2)	46.33	39.49	43.48	45.39
Robust BN (5e-3)	29.50	36.38	44.36	46.71
Balanced BN (Ours)	24.71	29.96	29.00	30.24

Table 5: The performance of different normalization layers which only updates the statistics. The classification error on CIFAR10-C are reported.

Ablation & Additional Study

Effect of Individual Components: We investigate the effectiveness of proposed components in Tab. 4. Specifically, we first compare adaptation by updating batchnorm statistics. It is apparent that Balanced BN is substantially better than Robust BN (Yuan, Xie, and Li 2023) when separately applied. When a two branch self-training (teacher & student net) is applied, we witness a clear improvement from the direct testing baseline. However the improvement is less significant by combining self-training with Balanced BN. This is probably caused by over adaptation to testing domains causing poor generalization to continually changing domains. This negative impact is finally remedied by introducing a tri-net architecture (Anchored Loss) which helps regularize self-training to avoid over adaptation.

Comparing Batchnorm Layers: To evaluate the effectiveness of our proposed Balanced BN, we run forward pass for global and local class-imbalanced testing samples for multiple batch normalization modules proposed for real-world TTA, with results presented in Tab. 5. We observe our proposed Balanced BN outperforms others with a large margin (2.58 ~ 9.79%), especially under severely global class imbalance (*I.F.* = 200). It further confirms that Balanced BN is more suitable for handling both global and local class-imbalanced testing data.

Hyper-parameter Robustness: Selecting appropriate hyper-parameter plays an important role in TTA (Zhao et al. 2023). As TTA assumes no labeled data in testing set, selecting appropriate hyper-parameter becomes non-trivial. We argue that the tri-net design is naturally more robust to the choice

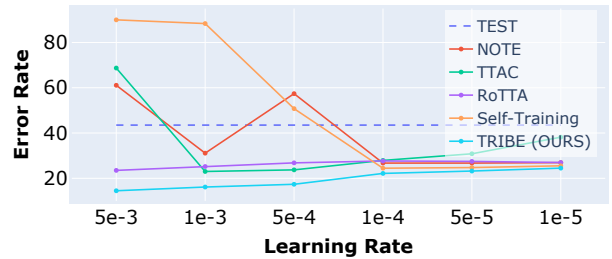


Figure 5: We evaluate state-of-the-art TTA methods under different learning rates. The learning rates of NOTE fall in [5e-4, 1e-6] and TTAC fall in [5e-5, 1e-7] in order to align the best LR with other methods.

of learning rate. As illustrated in Fig. 5, TRIBE is very stable w.r.t. the choice of learning rate while other methods, e.g. TTAC and NOTE, prefer a much narrower range of learning rate. More hyper-parameter analysis details can be found in the supplementary.

Conclusion

In this work, we explore improving test-time adaptation algorithm’s robustness to real-world challenges, including non-i.i.d. testing data stream, global class imbalance and continual domain shift. To adapt to imbalanced testing data, we propose a Balanced Batchnorm layer consisting of multiple category-wise statistics to achieve unbiased estimation of statistics. We further propose a tri-net architecture with student, teacher and anchor networks to regularize self-training based TTA. We demonstrate the effectiveness of the overall method, TRIBE, on simulated real-world test-time adaptation data streams. We achieve the state-of-the-art performance on all benchmarks created from four TTA datasets.

Limitations: TRIBE replaces regular Batchnorm layer with a customized Balanced Batchnorm layer, thus introducing additional storage overhead. Moreover, some recent Transformer based backbone network prefer Layernorm to Batchnorm (Dosovitskiy et al. 2021), thus potentially limiting the application of TRIBE. But recent studies revealed opportunities to integrate batchnorm to vision Transformer networks (Yao et al. 2021).

Acknowledgments

This work is supported by National Natural Science Foundation of China (NSFC) (Grant Number: 62106078), and Agency for Science, Technology and Research (Grant Number: C210112059). This work was partially done during Yongyi Su's attachment with Institute for Infocomm Research (I2R), funded by China Scholarship Council (CSC).

References

Arazo, E.; Ortego, D.; Albert, P.; O'Connor, N. E.; and McGuinness, K. 2020. Pseudo-labeling and confirmation bias in deep semi-supervised learning. In *International Joint Conference on Neural Networks*.

Boudiaf, M.; Mueller, R.; Ben Ayed, I.; and Bertinetto, L. 2022. Parameter-free Online Test-time Adaptation. In *Proceedings of the IEEE/CVF Conference on Computer Vision and Pattern Recognition*.

Brahma, D.; and Rai, P. 2023. A Probabilistic Framework for Lifelong Test-Time Adaptation. In *Proceedings of the IEEE/CVF Conference on Computer Vision and Pattern Recognition*, 3582–3591.

Chen, D.; Wang, D.; Darrell, T.; and Ebrahimi, S. 2022. Contrastive Test-Time Adaptation. In *Proceedings of the IEEE/CVF Conference on Computer Vision and Pattern Recognition*.

Croce, F.; Andriushchenko, M.; Sehwag, V.; Debenedetti, E.; Flammarion, N.; Chiang, M.; Mittal, P.; and Hein, M. 2021. RobustBench: a standardized adversarial robustness benchmark. In *Thirty-fifth Conference on Neural Information Processing Systems Datasets and Benchmarks Track (Round 2)*.

Cui, Y.; Jia, M.; Lin, T.-Y.; Song, Y.; and Belongie, S. 2019. Class-balanced loss based on effective number of samples. In *Proceedings of the IEEE/CVF Conference on Computer Vision and Pattern Recognition*.

Dosovitskiy, A.; Beyer, L.; Kolesnikov, A.; Weissenborn, D.; Zhai, X.; Unterthiner, T.; Dehghani, M.; Minderer, M.; Heigold, G.; Gelly, S.; Uszkoreit, J.; and Houlsby, N. 2021. An Image is Worth 16x16 Words: Transformers for Image Recognition at Scale. In *International Conference on Learning Representations*.

Gandelsman, Y.; Sun, Y.; Chen, X.; and Efros, A. A. 2022. Test-time training with masked autoencoders. In *Advances in Neural Information Processing Systems*.

Ganin, Y.; and Lempitsky, V. 2015. Unsupervised domain adaptation by backpropagation. In *International Conference on Machine Learning*.

Gong, T.; Jeong, J.; Kim, T.; Kim, Y.; Shin, J.; and Lee, S. 2022. Robust Continual Test-time Adaptation: Instance-aware BN and Prediction-balanced Memory. In *Advances in Neural Information Processing Systems*.

Goyal, S.; Sun, M.; Raghunathan, A.; and Kolter, J. Z. 2022. Test Time Adaptation via Conjugate Pseudo-labels. In *Advances in Neural Information Processing Systems*.

Gretton, A.; Borgwardt, K. M.; Rasch, M. J.; Schölkopf, B.; and Smola, A. 2012. A kernel two-sample test. *Journal of Machine Learning Research*.

He, K.; Zhang, X.; Ren, S.; and Sun, J. 2016. Deep residual learning for image recognition. In *Proceedings of the IEEE/CVF Conference on Computer Vision and Pattern Recognition*, 770–778.

Hendrycks, D.; and Dietterich, T. 2019. Benchmarking Neural Network Robustness to Common Corruptions and Perturbations. In *International Conference on Learning Representations*.

Hoffman, J.; Tzeng, E.; Park, T.; Zhu, J.-Y.; Isola, P.; Saenko, K.; Efros, A.; and Darrell, T. 2018. Cycada: Cycle-consistent adversarial domain adaptation. In *International Conference on Machine Learning*.

Ioffe, S.; and Szegedy, C. 2015. Batch normalization: Accelerating deep network training by reducing internal covariate shift. In *International Conference on Machine Learning*.

Iwasawa, Y.; and Matsuo, Y. 2021. Test-time classifier adjustment module for model-agnostic domain generalization. *Advances in Neural Information Processing Systems*, 34: 2427–2440.

Kingma, D. P.; and Ba, J. 2014. Adam: A method for stochastic optimization. *arXiv preprint arXiv:1412.6980*.

Kumar, A.; Ma, T.; and Liang, P. 2020. Understanding self-training for gradual domain adaptation. In *International Conference on Machine Learning*.

Lecun, Y.; Bottou, L.; Bengio, Y.; and Haffner, P. 1998. Gradient-based learning applied to document recognition. *Proceedings of the IEEE*, 86(11): 2278–2324.

Lee, D.-H.; et al. 2013. Pseudo-label: The simple and efficient semi-supervised learning method for deep neural networks. In *Workshop on challenges in representation learning, ICML*, volume 3, 896.

Lim, H.; Kim, B.; Choo, J.; and Choi, S. 2023. TTN: A domain-shift aware batch normalization in test-time adaptation. *arXiv preprint arXiv:2302.05155*.

Liu, H.; Wang, J.; and Long, M. 2021. Cycle self-training for domain adaptation. In *Advances in Neural Information Processing Systems*.

Liu, Y.; Kothari, P.; van Delft, B.; Bellot-Gurlet, B.; Mordan, T.; and Alahi, A. 2021. TTT++: When Does Self-Supervised Test-Time Training Fail or Thrive? In *Advances in Neural Information Processing Systems*.

Long, M.; Cao, Y.; Wang, J.; and Jordan, M. 2015. Learning transferable features with deep adaptation networks. In *International Conference on Machine Learning*.

Loshchilov, I.; and Hutter, F. ???? SGDR: Stochastic Gradient Descent with Warm Restarts. In *International Conference on Learning Representations*.

Mu, N.; and Gilmer, J. 2019. Mnist-c: A robustness benchmark for computer vision. *arXiv preprint arXiv:1906.02337*.

Nado, Z.; Padhy, S.; Sculley, D.; D'Amour, A.; Lakshminarayanan, B.; and Snoek, J. 2020. Evaluating Prediction-Time Batch Normalization for Robustness under Covariate Shift. *CoRR*, abs/2006.10963.

Niu, S.; Wu, J.; Zhang, Y.; Chen, Y.; Zheng, S.; Zhao, P.; and Tan, M. 2022. Efficient test-time model adaptation without

forgetting. In *International Conference on Machine Learning*.

Niu, S.; Wu, J.; Zhang, Y.; Wen, Z.; Chen, Y.; Zhao, P.; and Tan, M. 2023. Towards stable test-time adaptation in dynamic wild world. *International Conference on Learning Representations*.

Sakaridis, C.; Dai, D.; and Van Gool, L. 2018. Semantic foggy scene understanding with synthetic data. *International Journal of Computer Vision*.

Sohn, K.; Berthelot, D.; Carlini, N.; Zhang, Z.; Zhang, H.; Raffel, C. A.; Cubuk, E. D.; Kurakin, A.; and Li, C.-L. 2020. Fixmatch: Simplifying semi-supervised learning with consistency and confidence. *Advances in Neural Information Processing Systems*.

Su, Y.; Xu, X.; and Jia, K. 2022. Revisiting Realistic Test-Time Training: Sequential Inference and Adaptation by Anchored Clustering. In *Advances in Neural Information Processing Systems*.

Su, Y.; Xu, X.; Li, T.; and Jia, K. 2023. Revisiting Realistic Test-Time Training: Sequential Inference and Adaptation by Anchored Clustering Regularized Self-Training. *arXiv preprint arXiv:2303.10856*.

Sun, B.; and Saenko, K. 2016. Deep coral: Correlation alignment for deep domain adaptation. In *European Conference on Computer Vision*.

Sun, J.; Zhang, Q.; Kailkhura, B.; Yu, Z.; Xiao, C.; and Mao, Z. M. 2022. Benchmarking Robustness of 3D Point Cloud Recognition Against Common Corruptions. *arXiv preprint arXiv:2201.12296*.

Sun, Y.; Wang, X.; Liu, Z.; Miller, J.; Efros, A.; and Hardt, M. 2020. Test-time training with self-supervision for generalization under distribution shifts. In *International Conference on Machine Learning*.

Tang, H.; Chen, K.; and Jia, K. 2020. Unsupervised domain adaptation via structurally regularized deep clustering. In *Proceedings of the IEEE/CVF Conference on Computer Vision and Pattern Recognition*.

Tzeng, E.; Hoffman, J.; Zhang, N.; Saenko, K.; and Darrell, T. 2014. Deep domain confusion: Maximizing for domain invariance. *arXiv preprint arXiv:1412.3474*.

Wang, D.; Shelhamer, E.; Liu, S.; Olshausen, B. A.; and Darrell, T. 2021. Tent: Fully Test-Time Adaptation by Entropy Minimization. In *International Conference on Learning Representations*.

Wang, J.; Lan, C.; Liu, C.; Ouyang, Y.; Qin, T.; Lu, W.; Chen, Y.; Zeng, W.; and Yu, P. 2022a. Generalizing to unseen domains: A survey on domain generalization. *IEEE Transactions on Knowledge and Data Engineering*.

Wang, M.; and Deng, W. 2018. Deep visual domain adaptation: A survey. *Neurocomputing*.

Wang, Q.; Fink, O.; Gool, L. V.; and Dai, D. 2022b. Continual Test-Time Domain Adaptation. In *Proceedings of the IEEE/CVF Conference on Computer Vision and Pattern Recognition*.

Wu, R.; Guo, C.; Su, Y.; and Weinberger, K. Q. 2021. Online adaptation to label distribution shift. In *Advances in Neural Information Processing Systems*.

Xie, S.; Girshick, R.; Dollár, P.; Tu, Z.; and He, K. 2017. Aggregated residual transformations for deep neural networks. In *Proceedings of the IEEE/CVF Conference on Computer Vision and Pattern Recognition*, 1492–1500.

Yao, Z.; Cao, Y.; Lin, Y.; Liu, Z.; Zhang, Z.; and Hu, H. 2021. Leveraging batch normalization for vision transformers. In *Proceedings of the IEEE International Conference on Computer Vision*.

Yuan, L.; Xie, B.; and Li, S. 2023. Robust Test-Time Adaptation in Dynamic Scenarios. In *Proceedings of the IEEE/CVF Conference on Computer Vision and Pattern Recognition*.

Zagoruyko, S.; and Komodakis, N. 2016. Wide Residual Networks. In *British Machine Vision Conference 2016*. British Machine Vision Association.

Zellinger, W.; Grubinger, T.; Lugofer, E.; Natschläger, T.; and Saminger-Platz, S. 2016. Central moment discrepancy (cmd) for domain-invariant representation learning. In *International Conference on Learning Representations*.

Zhang, Y.; Hooi, B.; Hong, L.; and Feng, J. 2022. Self-supervised aggregation of diverse experts for test-agnostic long-tailed recognition. In *Advances in Neural Information Processing Systems*.

Zhao, H.; Liu, Y.; Alahi, A.; and Lin, T. 2023. On Pitfalls of Test-Time Adaptation. In *ICLR 2023 Workshop on Pitfalls of limited data and computation for Trustworthy ML*.

Appendix of "Towards Real-World Test-Time Adaptation: Tri-Net Self-Training with Balanced Normalization"

In this supplementary material, we first review the real-world test-time adaptation evaluation protocols and highlight the challenges arising from the proposed TTA protocol. We further present evaluations on MNIST-C dataset and demonstrate that TRIBE achieves the state-of-the-art performance. Next, we provide more in-depth evaluations into individual components, more fine-grained evaluations of different degrees of class-imbalance and detailed evaluations of sensitivity to hyper-parameters. Related works about test-time strategies are discussed. Eventually, we present a derivation for the proposed Balanced BN layer, details for data augmentation adopted in self-training and more detailed results on each type of corruption across all datasets.

Details of real-world TTA protocols

We aim to simulate a real-world test-time adaptation protocol by considering three key factors, namely non-stationary domain shift, imbalanced local class distribution and imbalanced global class distribution. First of all, we compare the challenging real-world TTA protocol against existing evaluation protocols in Tab. 6. The “Fully Test-Time Adaptation” (Wang et al. 2021; Su, Xu, and Jia 2022) makes the strongest assumption on the testing data stream by assuming a static testing domain shift and balanced class distribution both locally and globally. “Continual Test-Time Adaptation” (Wang et al. 2022b) further advances towards a more realistic TTA protocol by allowing testing domain to shift over time. “Non-i.i.d. Test-Time Adaptation” (Gong et al. 2022) further proposed a protocol simulating the testing data stream drawn in a non-i.i.d. manner from different classes, resulting imbalanced class distribution within a local time window. “Practical Test-Time Adaptation” (Yuan, Xie, and Li 2023) combines the above two real challenges together which poses more challenges to existing TTA methods. Finally, we would like to consider additionally that the global class distribution on the testing data stream could be imbalanced and introduce two variants of real-world TTA protocols for Global and Local class Imbalanced Test Time Adaptation (GLI-TTA), namely “GLI-TTA-F” and “GLI-TTA-V”, to mimic the most difficult testing data stream. In particular, “GLI-TTA-F” assumes the global class distribution is fixed over the whole testing data stream while “GLI-TTA-V” allows the global class distribution to vary over time. The more specific comparisons of different TTA protocols are presented in Tab. 6.

Global Class-Imbalance

In this section, we show the class distributions under different GLI-TTA protocols on CIFAR10-C and CIFAR100-C in Fig. 6 and Fig. 7 respectively. We follow the strategy proposed in (Cui et al. 2019) to generate imbalanced testing data stream. Specifically, we define the proportion parameter as $\alpha_k = \sigma \cdot (\frac{1}{I.F.})^{k/K_c}$, where σ controls the degree of local

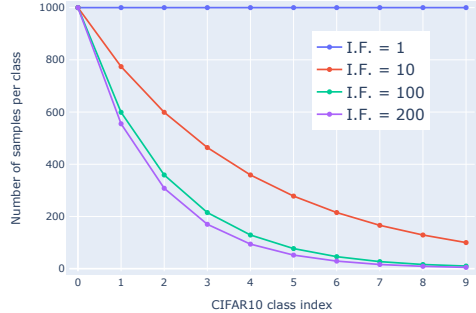


Figure 6: The number of testing samples per class in each domain (type of corruption) on CIFAR10-C under different imbalance degrees of GLI-TTA protocols.

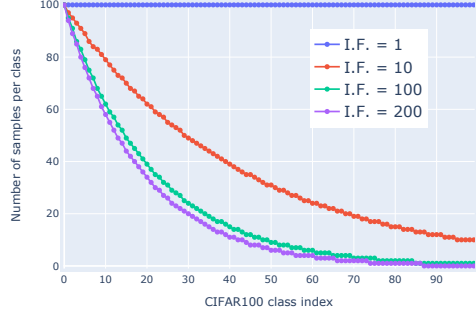


Figure 7: The number of testing samples per class in each domain (type of corruption) on CIFAR100-C under different imbalance degrees of GLI-TTA protocols.

class-imbalance, $I.F.$ denotes the imbalanced factor and k refers to the index of semantic category.

Additional Evaluation

Evaluation on MNIST-C

MNIST-C (Mu and Gilmer 2019) is constructed by injecting simulated corruptions to the testing set of MNIST (Le-cun et al. 1998). MNIST-C includes 15 types of corruptions to the digit images, consisting of Shot Noise, Impulse Noise, Glass Blur, Motion Blur, Shear, Scale, Rotate, Brightness, Translate, Stripe, Fog, Spatter, Dotted Line, Zigzag, and Canny Edges. Each corruption set has 10,000 testing samples divided into 10 categories. We train a ResNet18 (He et al. 2016) on clean MNIST training set for 100 epochs, using Adam (Kingma and Ba 2014) with initialized learning rate $1e-3$ and cosine annealing learning rate scheduling (Loshchilov and Hutter). The pre-trained model is used for test-time adaptation on MNIST-C testing set under GLI-TTA protocols. To simulate continually shifting domains, we adopt a domain (corruption) shifting order as “*ShotNoise* → *ImpulseNoise* → *GlassBlur* →

Setting	Stationary Domain	Balanced Local Class Distribution	Global Class Distribution
Fully Test-Time Adaptation (Wang et al. 2021)	✓	✓	Balanced
Continual Test-Time Adaptation (Wang et al. 2022b)	✗	✓	Balanced
Non-i.i.d. Test-Time Adaptation (Gong et al. 2022)	✓	✗	Balanced
Practical Test-Time Adaptation (Yuan, Xie, and Li 2023)	✗	✗	Balanced
GLI-TTA-F (Ours)	✗	✗	Imbalanced & Fixed
GLI-TTA-V (Ours)	✗	✗	Imbalanced & Varying

Table 6: Comparing existing real-world TTA protocols with our proposed GLI-TTA protocols

Method	Fixed Global Class Distribution (GLI-TTA-F)			
	<i>I.F.</i> = 1	<i>I.F.</i> = 10	<i>I.F.</i> = 100	<i>I.F.</i> = 200
TEST	14.52 / 14.53	15.10 / 14.57	15.63 / 14.64	15.73 / 14.25
BN (Nado et al. 2020)	63.76 / 63.75	61.27 / 54.48	61.15 / 39.31	61.42 / 35.27
PL (Lee et al. 2013)	67.58 / 67.55	62.65 / 55.89	61.94 / 40.35	60.73 / 35.83
TENT (Wang et al. 2021)	70.60 / 70.55	64.51 / 57.91	61.12 / 40.91	60.53 / 35.80
LAME (Boudiaf et al. 2022)	12.69 / 12.70	13.44 / 12.81	14.07 / 13.88	14.25 / 14.71
NOTE (Gong et al. 2022)	10.08 / 10.04	11.73 / 9.92	15.02 / 10.50	14.67 / 10.06
TTAC (Su, Xu, and Jia 2022)	13.02 / 13.03	15.10 / 14.48	15.43 / 14.60	15.48 / 14.20
RoTTA (Yuan, Xie, and Li 2023)	7.62 / 7.60	8.94 / 8.41	11.28 / 10.36	11.31 / 9.53
TRIBE	7.60 / 7.58	8.11 / 8.11	8.30 / 8.02	8.22 / 7.14

Method	Time-Varying Global Class Distribution (GLI-TTA-V)			
	<i>I.F.</i> = 1	<i>I.F.</i> = 10	<i>I.F.</i> = 100	<i>I.F.</i> = 200
TEST	14.52 / 14.53	12.42 / 14.68	10.60 / 14.13	10.31 / 14.07
BN (Nado et al. 2020)	63.76 / 63.75	58.65 / 53.88	56.79 / 37.25	57.08 / 34.25
PL (Lee et al. 2013)	67.58 / 67.55	61.05 / 55.95	58.35 / 38.45	58.06 / 34.62
TENT (Wang et al. 2021)	70.60 / 70.55	62.00 / 57.33	59.10 / 39.18	59.28 / 36.00
LAME (Boudiaf et al. 2022)	12.69 / 12.70	10.47 / 12.94	8.69 / 13.46	8.25 / 13.87
NOTE (Gong et al. 2022)	10.08 / 10.04	9.30 / 9.15	9.18 / 9.02	9.01 / 8.88
TTAC (Su, Xu, and Jia 2022)	13.02 / 13.03	12.15 / 14.32	10.46 / 14.09	10.18 / 14.09
RoTTA (Yuan, Xie, and Li 2023)	7.62 / 7.60	8.45 / 8.62	9.33 / 9.22	9.74 / 9.48
TRIBE	7.60 / 7.58	8.28 / 8.11	8.28 / 7.39	8.77 / 8.01

Table 7: Average classification error (lower the better) on MNIST-C while continually adapting to different corruptions with globally and locally class-imbalanced test stream. *I.F.* is the Imbalance Factor of Global Class-Imbalance. Instance-wise average error rate *a*% and category-wise average error rate *b*% are separated by (a / b).

MotionBlur → *Shear* → *Scale* → *Rotate* → *Brightness* → *Translate* → *Stripe* → *Fog* → *Spatter* → *DottedLine* → *Zigzag* → *CannyEdges*”. Quantitative results are shown in Tab. 7. We make the similar observations with the results on CIFAR10/100-C and ImageNet-C evaluated in the manuscript as below. i) Some test-time adaptations (e.g., BN, PL and TENT) obtain worse results than without adaptation, which demonstrates it’s necessary to propose a more robust test-time adaptation method which can better handle different kinds of test streams. ii) Our proposed **TRIBE** consistently outperforms other competing methods in both challenging GLI-TTA protocols.

The effectiveness of individual components under non-i.i.d. TTA protocol

In this section, we provide an in-depth comparative study of the individual components used in RoTTA (Yuan, Xie, and Li 2023) and our proposed **TRIBE**. We follow the PTTA protocol defined in (Yuan, Xie, and Li 2023) by evaluating on CIFAR10-C with local class-imbalance and continual domain shift. Specifically, we analyze the components including i) exponentially moving average model (EMA Model), ii) category-balanced memory (Yuan, Xie, and Li 2023), iii) Robust BN (Yuan, Xie, and Li 2023), iv) Balanced BN, v) consistency constraint or self-training loss (Consis. Const. / ST Loss) and vi) anchored loss. From the results shown in Tab. 8, we observe that, i) comparing lines 2 and 9, our proposed Balanced BN outperforms the combination of category-balanced memory and Robust BN (25.2% → 21.6%), which demon-

Line	Method	Component						Avg. Error Rate
		EMA Model	Category-balanced Memory (Yuan, Xie, and Li 2023)	Robust BN (Yuan, Xie, and Li 2023)	Balanced BN	Consis. Const. / ST Loss	Anchored Loss	
1	TEST	–	–	–	–	–	–	43.5
2	RoTTA (Yuan, Xie, and Li 2023)	✓	✓	✓	–	✓	–	25.2
3	–	–	✓	✓	–	✓	–	58.5
4	–	–	✓	✓	–	✓	✓	25.5
5	–	–	✓	–	✓	✓	✓	25.0
6	–	–	–	✓	–	✓	–	46.0
7	–	–	–	✓	–	✓	✓	40.3
8	–	–	–	✓	–	✓	–	44.1
9	Mean Teacher*	✓	–	–	✓	✓	–	21.6
10	–	✓	✓	–	✓	✓	–	23.3
11	FixMatch*	–	–	–	✓	✓	–	88.4
12	–	–	–	–	–	✓	✓	34.9
13	Robust BN (Yuan, Xie, and Li 2023)	–	–	✓	–	–	–	46.3
14	Balanced BN	–	–	–	✓	–	–	24.7
15	TRIBE	–	–	–	✓	✓	✓	16.1

Table 8: Analysis of individual components. Consis. Const. indicates Consistency Constraint. The **bold** text indicates our contributed module. Mean Teacher* and FixMatch* are adapted to TTA task by removing the labeled loss term.

strates the effectiveness of our proposed Balanced BN under local class-imbalance. Although RoTTA tries to smooth the impact from non-i.i.d. data through memory bank and robust batchnorm, memory bank highly depends on the pseudo labels and the label-inaccurate samples would be accumulated in the memory. In our proposed **TRIBE**, we abandon the memory bank and adapt the non-i.i.d. test streaming data by our proposed Balanced BN, which demonstrates strong capability in adapting to locally imbalanced testing data stream. ii) Compared with line 3, the approach with our proposed Anchored Loss (line 4) achieves better performance. The similar observation, e.g., lines 6 and 7, also demonstrates the effectiveness of Anchored Loss. iii) In addition to the positive results above, we observe only combining Balanced BN and ST Loss (line 11) causes a bad result. We hypothesize that it is due to the confirmation bias accumulation and over-adaptation caused by only performing ST Loss without Anchored Loss and this gradually severe confirmation bias in turn affects the Balanced BN. Fortunately, this negative impact is finally remedied by introducing Anchored Loss (**TRIBE** line 15).

Evaluation on gradually changing corruptions.

To simulate such a non-stationary corruption severity we carried out an experiment by repeating TTA on the testing data stream 5 times with an increasing corruption severity from 1 to 5. Both local and global class-imbalance, GLI-TTA-F (IF=100), are simulated in this scenario. As shown in Tab. 9, TRIBE still outperforms all competing methods with a large margin under non-stationary corruption severity.

Avg Error	TEST	BN	TENT	CoTTA	RoTTA	TRIBE
CIFAR10C	22.89	67.31	74.75	75.78	20.18	10.49

Table 9: TTA performance on CIFAR10-C under gradually changing corruption severity. Both local and global class-imbalance, i.e. GLI-TTA-F (IF=100), are simulated in the experiment.

Computation Cost Measured in Wall-Clock Time

We evaluate the computation cost of our proposed TRIBE in this section. It's worthy note that, we only update the weight

and bias parameters in batchnorm layers so that most of parameters across three models are shared, with only a small fraction of the remaining independent parameters. On the other hand, we have implemented Balanced BN as efficiently as possible using cpp in order to make the algorithm more efficient and more effective. Here, we provide the computation cost analysis of our TRIBE and several SOTA TTA methods in Tab. 10. We make the following observations. Our model undeniably got the best result and by a huge margin with others, and our model didn't take too much extra time compared to other SOTAs (only 1ms more than ROTTA), which we feel is acceptable for a TTA method.

Method	Error Rate	Inference and Adaptation Time per Sample (second)
TEST	41.71	0.0005
BN	70.00	0.0005
TENT	71.10	0.0009
NOTE	42.59	0.0020
COTTA	71.32	0.0190
TTAC (w/o queue)	43.40	0.0021
PETAL	71.14	0.0163
ROTTA	30.50	0.0033
TRIBE	19.53	0.0043

Table 10: The per-sample wall time (measured in seconds) on CIFAR10-C under GLI-TTA-F (IF=100) protocol.

The robustness of TRIBE under more fine-grained degrees of global class-imbalance under GLI-TTA-F protocol

We evaluate TRIBE on more fine-grained degrees of global class-imbalance under GLI-TTA-F protocol and show the instance-level average classification error rates on Tab. 11. We choose the global imbalance factor as 1, 2, 4, 8, 10, 40, 80, 100 and 200. The results demonstrate the robustness and stability of our proposed **TRIBE** on different global class-imbalanced degrees, and the performance varies between 16.10% and 20.98%.

I.F.	1	2	4	8	10	20	40	80	100	200
TRIBE	16.10	18.97	20.15	20.96	20.98	20.63	20.01	19.37	19.53	19.16

Table 11: More detailed results under different global class-imbalance factors on CIFAR10-C under GLI-TTA-F protocol. The instance-level average error rates are reported.

The robustness of TRIBE under different degrees of local class-imbalance under practical TTA protocol

We evaluate TRIBE on different degrees of local class-imbalance. The comparisons between RoTTA (Yuan, Xie, and Li 2023) and our proposed **TRIBE** on three datasets (i.e. CIFAR10-C, CIFAR100-C and ImageNet-C) are shown in Tab. 12. We make the following observations. First, our proposed **TRIBE** consistently outperforms RoTTA on all datasets at all degrees of local class-imbalance. Second, with σ becoming smaller, the local class-imbalance is becoming more severe, but **TRIBE** is still able to maintain the performance on CIFAR10-C while RoTTA becomes substantially worse. This is probably attributed to the ability to welll balance between self-training loss with strong adaptive ability and anchored loss with stable regularized ability. Third, **TRIBE** has smaller performance fluctuations with the changing of local class-imbalance degrees, suggesting the robustness of TRIBE due to more sophisticated Balanced BN layer and tri-net architecture.

Dataset	Method	i.i.d.				non - i.i.d.
		10.	1.0	0.1	0.01	
CIFAR10-C	RoTTA	20.45	21.15	25.20	28.69	29.11
	TRIBE	19.91 ^(+0.54)	19.88 ^(+1.27)	16.14 ^(+9.06)	14.47 ^(+14.22)	12.39 ^(+16.72)
CIFAR100-C	RoTTA	33.90	34.00	35.00	38.20	40.14
	TRIBE	32.69 ^(+1.21)	32.93 ^(+1.07)	33.26 ^(+1.74)	34.50 ^(+3.70)	36.02 ^(+4.12)
ImageNet-C	RoTTA	66.70	66.81	66.90	67.20	67.33
	TRIBE	61.84 ^(+4.86)	62.53 ^(+4.28)	62.32 ^(+4.58)	63.02 ^(+4.18)	63.33 ^(+4.00)

Table 12: Average classification errors of different local class-imbalance degrees σ on three datasets. non-i.i.d. indicates more correlated testing data stream which results in local class-imbalance. i.i.d. indicates the neighborhood samples are sampled from i.i.d. distribution.

Sensitivity analysis of hyper-parameters used in TRIBE

Sensitivity of the balancing parameter γ in Balanced BN: To evaluate the sensitiveness of γ , we conduct the experiments on GLI-TTA-F (*I.F.* = 100) protocols on CIFAR10-C and CIFAR100-C. We show the performance from $\gamma = 0.0$ to $\gamma = 1.0$ in Tab. 13. Specifically, $\gamma = 1.0$ indicates the Balanced BN (class-wise statistics) degenerates to Robust BN (class-agnostic statistics). In this work, we choose $\gamma = 0.0$ on CIFAR10-C and $\gamma = 0.1$ on CIFAR100-C dataset. Additionally, we observe that, on CIFAR10-C dataset, when $\gamma = 1.0$ the performance degrades severely (Inst. Avg.: 19.53% \rightarrow 43.26%) and it demonstrates the class-agnostic batch norm is sensitive and vulnerable to test data stream with severe global and local class-imbalance. On CIFAR100-C dataset, the degradation is relatively mild (Inst. Avg.: 32.31% \rightarrow 33.26%) and this is probably caused by the fact that the number of testing samples per class on CIFAR100-C is much smaller than that on CIFAR10-C test set (shown in Fig. 6 and Fig. 7).

Sensitivity to the thresholding parameter H_0 in Tri-Net Self-Training: To evaluate the sensitiveness of H_0 , we conduct the experiments on GLI-TTA-F (*I.F.* = 100) protocols on CIFAR10-C and CIFAR100-C. We show the

performance from $H_0 = 0.0$ to $H_0 = 0.4$ in Tab. 14. In this work, we choose $H_0 = 0.05$ on CIFAR10-C and $H_0 = 0.20$ on CIFAR100-C for the experiments conducted on the manuscript. The H_0 is the hyper-parameter used in Tri-Net Self-Training module and aims to filter the high reliable pseudo labels for the stably adaptation process. This hyper-parameter is highly related to the accuracy on the original dataset (e.g. clean test set), yet we found the performance is continuous and robust from $H_0 = 0.05$ to $H_0 = 0.40$ on both CIFAR10-C and CIFAR100-C datasets.

Sensitivity to λ_{anc} : To evaluate the sensitiveness of λ_{anc} , we conduct the experiments on GLI-TTA-F (*I.F.* = 100) protocols on CIFAR10-C and CIFAR100-C. We show the performance from $\lambda_{anc} = 0.0$ to $\lambda_{anc} = 2.0$ in Tab. 15. λ_{anc} is the hyper-parameter balancing \mathcal{L}_{st} and \mathcal{L}_{anc} , where \mathcal{L}_{st} provides the strong adaptation ability to the specific domain but it easily causes the accumulated confirmation bias and over-confident issue (Arazo et al. 2020; Su et al. 2023) and \mathcal{L}_{anc} provides the regularization constraint to self-training. We choose $\lambda_{anc} = 0.5$ on all experiments of the manuscript. We observe that without \mathcal{L}_{anc} ($\lambda_{anc} = 0.$) the performance degrades from 19.53% to 36.58% on CIFAR10-C and from 32.31% to 37.21% on CIFAR100-C which demonstrates the important role of the anchored loss \mathcal{L}_{anc} .

Sensitivity to η : To evaluate the sensitivenss of η , we conduct the experiments on GLI-TTA-F (*I.F.* = 100) protocols on CIFAR10-C and CIFAR100-C. We show the performance from $\eta = 5e - 5 \times K_c$ to $\eta = 1e - 2 \times K_c$ in Tab. 16.

Related Work

Test-time Strategies

- (Wu et al. 2021) proposed Online gradient descent and Follow The History algorithms to adapt model to handle the label shift appearing at test time. However, there is no domain shift considered between training and test set. There's no denying these are great methods but it would make the pseudo labels (gradient direction from minimizing entropy) untrustworthy when the domain is changed.
- (Zhang et al. 2022) adopted three expert models, which supervised by three different losses, to learn from the same long-tailed source data in order to fuse them to deal with unknown test class distributions. However, the difficulties in TTA are i) the source model is pretrained in advance and we can not utilize the source domain to again train multiple expert models to deal with some test distributions, ii) training in long tailed source data with GT labels is different from fine-tuning models in long tailed test data with pseudo labels, since self-training with pseudo labels would easily accumulate confirmation bias without the regularization from GT labels.

In this paper, we mainly address the problem that given a pretrained source model (No special treatment for the test environment, generic model), we need to adapt it into a more realistic test scenario which fuses locally and globally class imbalanced testing data and the test environment (corruptions) is time-varying. Unlike reweighting strategy used into

Dataset	Error Rate	1.0	0.9	0.8	0.7	0.6	0.5	0.4	0.3	0.2	0.1	0.0 (Robust BN)
CIFAR10-C	Inst. Avg.	19.53	20.33	21.35	21.87	22.71	23.69	24.40	25.60	26.74	29.02	43.26
	Cat. Avg.	24.66	24.19	24.51	24.36	24.33	24.82	24.63	25.23	25.51	25.99	31.49
CIFAR100-C	Inst. Avg.	32.98	32.31	32.85	32.71	32.69	32.58	32.61	32.72	32.67	32.80	33.26
	Cat. Avg.	35.17	34.98	35.03	35.06	35.03	35.18	35.39	35.49	35.74	35.52	35.54

Table 13: The analysis about sensitivity to hyper-parameter $1 - \gamma$. The classification error rates are reported on CIFAR10-C and CIFAR100-C datasets under GLI-TTA-F ($I.F. = 100$) protocol.

Dataset	Error Rate	0.05	0.10	0.15	0.20	0.25	0.30	0.35	0.40
CIFAR10-C	Inst. Avg.	19.53	20.00	20.15	20.14	20.54	20.63	20.96	20.96
	Cat. Avg.	24.66	24.50	24.56	24.50	24.79	24.57	24.57	24.50
CIFAR100-C	Inst. Avg.	33.35	32.60	32.53	32.31	32.36	32.42	32.11	32.53
	Cat. Avg.	35.30	35.96	34.92	34.98	35.34	35.35	34.79	35.02

Table 14: The sensitive analysis about hyper-parameter H_0 . The classification error rates are reported on CIFAR10-C and CIFAR100-C datasets under GLI-TTA-F ($I.F. = 100$) protocol.

Dataset	Error Rate	0.0	0.5	1.0	1.5	2.0
CIFAR10-C	Inst. Avg.	36.58	19.53	21.94	23.23	24.32
	Cat. Avg.	65.88	24.66	24.52	24.43	24.69
CIFAR100-C	Inst. Avg.	37.21	32.31	33.93	34.95	35.53
	Cat. Avg.	44.83	34.98	34.92	35.18	35.17

Table 15: The sensitive analysis about hyper-parameter λ_{anc} . The classification error rates are reported on CIFAR10-C and CIFAR100-C datasets under GLI-TTA-F ($I.F. = 100$) protocol.

Dataset	$5e - 5 \times K_c$	$5e - 4 \times K_c$	$5e - 3 \times K_c$	$1e - 2 \times K_c$
CIFAR10-C	34.04	19.53	22.73	26.04
CIFAR100-C	45.57	32.31	32.66	32.85

Table 16: The sensitive analysis about hyper-parameter η . The classification error rates are reported on CIFAR10-C and CIFAR100-C datasets under GLI-TTA-F ($I.F. = 100$) protocol.

long-tailed tasks, e.g. Balanced Softmax, we propose the Balanced BatchNorm to alleviate the estimation bias of statistics maintained in batchnorm layers, and propose Anchor Network with Anchored Loss to alleviate the confirmation bias of learnable parameters updated by self-training loss.

Derivation of μ_g and σ_g^2 in Balanced BN

Balanced BN aims to obtain the class-balanced global distribution according to testing samples consisting of different numbers of samples from different category-wise distributions. Here, we provide the derivation of Balanced BN motivated by imbalanced testing data stream. We first assume that the testing samples $\{\mathbf{x}_i\}_{i=1 \dots N}$ consists of K_c categories of $\{\mathbf{x}_{k,i}\}_{i=1 \dots N_k}$, where N_k denotes the number of samples belonging to class k . We denote the k^{th} categorical distribution as $\{\mu_k, \sigma_k^2\}$. The class-agnostic global distribution $\{\mu_g, \sigma_g^2\}$ in a regular normalization layer (e.g. BN (Ioffe and Szegedy 2015)) can be obtained as Eq. 7 and Eq. 8.

$$\mu_g = \frac{\sum_{i=1}^N \mathbf{x}_i}{N} = \frac{\sum_{k=1}^{K_c} \sum_{i=1}^{N_k} \mathbf{x}_{k,i}}{\sum_{k=1}^{K_c} N_k} = \frac{\sum_{k=1}^{K_c} N_k \mu_k}{\sum_{k=1}^{K_c} N_k}, \quad (7)$$

$$\begin{aligned} \sigma_g^2 &= \frac{\sum_{i=1}^N (\mathbf{x}_i - \mu_g)^2}{N} = \frac{\sum_{k=1}^{K_c} \sum_{i=1}^{N_k} (\mathbf{x}_{k,i} - \mu_g)^2}{\sum_{k=1}^{K_c} N_k} \\ &= \frac{1}{\sum_{k=1}^{K_c} N_k} \sum_{k=1}^{K_c} \sum_{i=1}^{N_k} (\mathbf{x}_{k,i} - \mu_k + \mu_k - \mu_g)^2 \\ &= \frac{1}{\sum_{k=1}^{K_c} N_k} \sum_{k=1}^{K_c} \sum_{i=1}^{N_k} (\mathbf{x}_{k,i} - \mu_k)^2 + (\mu_k - \mu_g)^2 \\ &\quad + 2(\mathbf{x}_{k,i} - \mu_k)(\mu_k - \mu_g) \\ &= \frac{\sum_{k=1}^{K_c} N_k [\sigma_k^2 + (\mu_k - \mu_g)^2]}{\sum_{k=1}^{K_c} N_k}. \end{aligned} \quad (8)$$

We can observe that the μ_g and σ_g^2 in regular BN tend to approximate to the distribution of the most majority class when the testing samples are severely class-imbalanced either locally or globally $\mu_g \approx \mu_{k'}, \sigma_g^2 \approx \sigma_{k'}^2$ s.t. $N_{k'} \approx N$, which would introduce a large bias to the model pre-trained on class-balanced source domain.

To mitigate the impact from the locally or globally class-imbalanced testing samples, we re-weight the category-wise distributions to obtain the class-balanced global distribution (denoted as $\{\mu_{ba}, \sigma_{ba}^2\}$) as Eq. 9 and Eq. 10.

$$\mu_{ba} = \frac{1}{K_c} \sum_{k=1}^{K_c} \frac{\sum_{i=1}^{N_k} \mathbf{x}_{k,i}}{N_k} = \frac{1}{K_c} \sum_{k=1}^{K_c} \mu_k \quad (9)$$

$$\begin{aligned} \sigma_{ba}^2 &= \frac{1}{K_c} \sum_{k=1}^{K_c} \frac{\sum_{i=1}^{N_k} (\mathbf{x}_{k,i} - \mu_{ba})^2}{N_k} \\ &= \frac{1}{K_c} \sum_{k=1}^{K_c} \frac{\sum_{i=1}^{N_k} (\mathbf{x}_{k,i} - \mu_k + \mu_k - \mu_{ba})^2}{N_k} \\ &= \frac{1}{K_c \cdot N_k} \sum_{k=1}^{K_c} \sum_{i=1}^{N_k} (\mathbf{x}_{k,i} - \mu_k)^2 + (\mu_k - \mu_{ba})^2 \\ &\quad + 2(\mathbf{x}_{k,i} - \mu_k)(\mu_k - \mu_{ba}) \\ &= \frac{1}{K_c} \sum_{k=1}^{K_c} [\sigma_k^2 + (\mu_k - \mu_{ba})^2] \end{aligned} \quad (10)$$

The formulas of μ_{ba} and σ_{ba} above demonstrate the ability of estimating the global class-balanced distribution using class-imbalanced testing samples due to the re-weighting strategy. We utilize the pseudo labels of testing samples to categorize them into K_c categories, and the pseudo labels are often predicted at the inference step of TTA.

Algorithm and implementation of Balanced BN

We provide an overview of the algorithm (Alg. 1) of Balanced BN in this section. An efficient implementation of Balanced BN using *Cpp* is also attached in the supplementary material.

Algorithm 1: The algorithm of Balanced BN

input : Input feature map $\mathbf{F} \in \mathbb{R}^{B \times C \times H \times W}$.
 Corresponding pseudo labels $\hat{\mathbf{Y}} \in \mathbb{R}^{B \times K_c}$.
output : Normalized feature map $\tilde{\mathbf{F}}$.
if *training* **then**
 | update $\{\mu_k\}_{k=1 \dots K_c}$ and $\{\sigma_k^2\}_{k=1 \dots K_c}$ according
 | to Eq. 3 of the manuscript.
 calculate μ_{ba} and σ_{ba}^2 according to Eq. 9 and Eq. 10.
 $\tilde{\mathbf{F}} = \alpha \frac{\mathbf{F} - \mu_{ba}}{\sqrt{\sigma_{ba}^2 + \epsilon}} + \beta$,
 where α and β here indicate the affine parameters of
 standard batchnorm module.
return $\tilde{\mathbf{F}}$

Data augmentations used in TRIBE

Data augmentation plays an important role in self-training. In this section, we provide more details of the data augmentation strategy adopted for the teacher model in TRIBE. The augmentation strategy is similar to the ones adopted in RoTTA (Yuan, Xie, and Li 2023). The data augmentations are including Clip, ColorJitter, Pad, RandomAffine and etc. The specific details can be found in the code provided into the supplementary materials.

Detail results under different GLI-TTA protocols

Finally, we present more detailed results for each dataset under the proposed TTA protocols.

Time		$t \rightarrow$															Inst.Avg.	Cat.Avg.
I.F.	Method	motion	snow	fog	shot	defocus	contrast	zoom	brightness	frost	elastic	glass	gaussian	pixelate	jpeg	impulse		
10	TEST	29.48	25.64	26.30	65.72	42.92	44.64	34.94	9.30	43.61	25.81	53.97	72.01	63.00	33.18	69.27	42.65	43.79
	BN (Nado et al. 2020)	66.04	70.30	68.90	72.38	69.17	68.83	68.54	65.60	68.24	74.49	75.44	73.14	69.78	74.80	75.91	70.77	66.77
	PL (Lee et al. 2013)	66.58	70.64	69.49	73.53	71.52	70.64	70.15	68.17	69.76	75.00	78.04	74.85	73.29	77.74	76.98	72.43	70.59
	TENT (Wang et al. 2021)	66.58	70.74	70.74	75.39	73.16	74.76	75.34	75.32	78.70	82.37	84.75	84.72	83.67	87.90	88.10	78.15	74.90
	LAME (Boudiaf et al. 2022)	23.70	19.81	20.67	65.48	37.73	41.53	29.16	5.73	39.45	17.70	50.32	71.96	61.51	24.85	67.16	38.45	40.07
	NOTE (Gong et al. 2022)	19.76	23.82	21.72	46.25	26.57	15.11	27.06	20.98	39.47	46.67	59.72	51.00	53.28	47.06	53.33	36.79	30.22
	TTAC (Su, Xu, and Jia 2022)	31.78	28.11	21.94	66.45	27.11	20.08	19.10	10.11	25.73	23.73	42.46	34.35	35.92	27.89	53.21	31.20	29.11
	RoTTA (Yuan, Xie, and Li 2023)	20.13	22.72	16.41	37.46	20.32	17.04	18.58	11.24	25.37	31.22	45.64	36.04	30.97	31.29	46.56	27.41	26.31
TRIBE		17.43	18.12	11.85	25.66	17.53	12.83	13.81	9.13	16.45	22.26	34.97	24.90	23.70	25.98	40.06	20.98 _(+6.43)	22.49 _(+3.82)
100	TEST	25.71	26.39	27.68	67.88	41.32	41.40	31.92	7.14	46.21	24.21	49.11	74.21	61.50	33.45	67.55	41.71	43.63
	BN (Nado et al. 2020)	64.77	69.09	68.16	72.48	68.89	67.64	63.96	62.47	65.78	72.92	75.50	74.86	71.51	74.66	77.28	70.00	50.72
	PL (Lee et al. 2013)	64.77	69.29	68.24	73.77	70.54	67.35	65.74	64.45	68.48	72.40	75.95	73.77	69.33	72.32	74.90	70.09	55.29
	TENT (Wang et al. 2021)	64.81	68.60	67.19	72.28	69.05	67.68	65.54	64.81	67.88	73.33	77.00	77.16	73.85	78.93	78.41	71.10	58.59
	LAME (Boudiaf et al. 2022)	20.10	19.65	21.95	67.84	36.64	37.77	25.14	3.75	42.49	16.67	44.75	74.29	60.17	25.34	65.70	37.48	41.80
	NOTE (Gong et al. 2022)	21.31	27.28	28.13	52.18	31.36	17.35	30.67	21.67	46.13	54.24	66.95	62.31	55.73	57.79	65.78	42.59	30.75
	TTAC (Su, Xu, and Jia 2022)	40.96	48.59	31.56	77.60	47.18	31.80	24.05	13.44	44.75	31.03	46.53	58.64	42.62	33.41	78.81	43.40	37.37
	RoTTA (Yuan, Xie, and Li 2023)	22.40	31.19	21.71	44.51	27.56	14.89	23.33	10.13	26.96	32.69	44.87	41.53	34.22	31.76	49.68	30.50	29.08
TRIBE		17.43	20.34	12.11	28.17	17.59	11.38	11.50	6.82	15.50	18.85	29.54	23.69	24.78	24.37	30.91	19.53 _(+10.97)	24.66 _(+4.42)
TRIBE		17.16	18.99	10.46	31.77	18.01	10.72	11.39	7.10	14.34	18.72	29.31	21.49	23.19	23.68	31.10	19.16 _(+13.29)	24.00 _(+6.04)

Table 17: Average classification error on CIFAR10-C while continually adapting to different corruptions at the highest severity 5 with globally and locally class-imbalanced test stream and fixed global class distribution (GLI-TTA-F). *I.F.* is the Imbalanced Factor of Global Class-Imbalance.

Time		$t \rightarrow$															Inst.Avg.	Cat.Avg.
I.F.	Method	motion	snow	fog	shot	defocus	contrast	zoom	brightness	frost	elastic	glass	gaussian	pixelate	jpeg	impulse		
10	TEST	30.06	40.25	51.60	69.32	29.95	55.60	28.97	29.57	47.21	36.89	54.10	73.68	76.70	41.23	39.27	46.96	46.52
	BN (Nado et al. 2020)	39.99	46.44	52.48	49.95	39.81	41.10	39.29	37.93	46.16	46.67	51.01	52.66	44.76	50.75	51.75	46.05	42.29
	PL (Lee et al. 2013)	40.12	46.47	55.01	57.17	54.15	60.71	62.82	64.01	71.18	77.63	83.67	85.17	85.84	90.61	93.06	68.51	69.71
	TENT (Wang et al. 2021)	39.16	45.28	53.82	61.76	63.39	76.37	78.25	83.38	89.50	91.49	93.52	92.96	93.94	95.23	95.18	76.88	79.08
	LAME (Boudiaf et al. 2022)	26.08	34.80	48.35	68.99	24.59	54.77	23.66	24.61	43.70	31.09	50.77	73.81	78.22	36.56	34.93	43.66	44.88
	NOTE (Gong et al. 2022)	44.94	51.50	58.82	62.95	47.88	40.66	49.23	47.50	55.57	60.50	67.44	66.77	63.98	70.10	77.84	57.71	58.86
	TTAC (Su, Xu, and Jia 2022)	28.87	41.28	46.65	56.01	33.69	44.53	31.76	29.44	40.09	37.33	43.42	50.88	46.08	42.23	34.91	40.48	38.28
	RoTTA (Yuan, Xie, and Li 2023)	33.88	42.00	47.01	49.74	35.37	46.16	35.73	27.09	39.58	39.99	41.59	42.05	37.15	38.98	43.73	40.00	39.03
TRIBE		28.35	33.13	38.83	39.11	28.33	27.84	26.68	24.64	31.22	33.23	37.44	39.65	33.26	36.38	38.42	33.10 _(+6.90)	34.31 _(+3.97)
100	TEST	29.80	42.05	50.96	69.45	31.39	55.84	29.28	30.17	49.18	37.45	54.20	75.04	77.66	41.11	39.37	47.53	45.91
	BN (Nado et al. 2020)	40.69	47.30	54.76	51.20	40.22	42.05	40.22	39.93	47.49	47.96	51.76	51.10	45.28	53.26	51.95	47.01	40.01
	PL (Lee et al. 2013)	40.26	45.75	50.82	49.32	44.39	47.16	44.91	46.08	52.28	54.81	60.72	64.38	62.08	68.61	70.30	53.46	57.26
	TENT (Wang et al. 2021)	38.90	42.23	45.75	46.88	42.23	48.57	46.97	51.15	59.27	63.02	67.95	72.08	72.13	76.40	77.29	56.72	65.96
	LAME (Boudiaf et al. 2022)	25.53	36.37	46.88	68.84	25.86	54.95	23.98	24.50	46.27	31.53	50.59	75.74	79.02	35.95	36.32	44.15	46.64
	NOTE (Gong et al. 2022)	44.53	50.40	58.94	65.27	46.45	39.80	45.57	43.36	50.16	54.95	62.04	64.34	58.61	63.12	69.50	54.44	57.10
	TTAC (Su, Xu, and Jia 2022)	31.11	52.28	52.37	61.10	36.88	53.73	32.75	33.18	49.23	43.97	45.71	60.63	66.64	54.34	43.74	47.84	41.47
	RoTTA (Yuan, Xie, and Li 2023)	35.05	46.27	51.10	57.72	42.05	40.36	45.89	28.63	49.27	50.45	46.03	50.45	48.33	46.93	46.69	45.68	42.04
TRIBE		27.08	34.02	38.06	41.20	29.94	28.25	26.70	23.51	30.78	31.44	34.58	37.45	33.18	34.73	33.79	32.31 _(+11.84)	34.98 _(+5.82)
200	TEST	29.86	41.30	50.54	69.71	30.99	56.39	29.22	30.72	49.68	37.92	54.51	74.87	77.82	41.14	39.26	47.59	39.94
	BN (Nado et al. 2020)	41.46	47.48	53.76	52.31	40.33	43.02	41.41	40.33	47.42	47.69	52.09	51.02	44.58	54.78	53.01	47.38	35.26
	PL (Lee et al. 2013)	41.35	43.72	47.80	48.01	39.69	44.36	41.62	39.96	48.07	50.27	55.96	57.30	54.51	64.45	64.07	49.41	49.26
	TENT (Wang et al. 2021)	39.42	42.00	45.76	44.58	39.53	43.02	40.01	42.32	49.14	54.19	59.72	60.96	58.11	67.51	70.46	50.45	58.45
	LAME (Boudiaf et al. 2022)	25.46	34.91	46.46	68.74	25.46	54.46	23.36	23.90	45.38	31.69	51.07	75.56	79.86	35.39	35.45	43.81	40.33
	NOTE (Gong et al. 2022)	44.95	50.27	59.67	63.48	46.19	37.65	45.44	43.72	50.48	54.83	61.82	61.49	57.84	61.06	67.19	53.74	52.48
	TTAC (Su, Xu, and Jia 2022)	32.44	54.19	55.26	62.62	37.00	55.21	33.57	34.00	51.93	46.19	47.05	61.60	70.89	56.02	48.71	49.78	38.00
	RoTTA (Yuan, Xie, and Li 2023)	34.21	46.13	51.72	58.59	42.21	41.62	46.29	28.95	49.73	57.47	47.80	51.50	49.46	48.98	47.05	46.78	37.93
TRIBE		27.34	32.17	37.38	40.01	30.50	29.38	27.28	23.58	30.45	32.55	34.91	36.41	35.82	33.73	32.81	32.29 _(+11.52)	31.54 _(+3.72)

Table 18: Average classification error on CIFAR100-C while continually adapting to different corruptions at the highest severity 5 with globally and locally class-imbalanced test stream and fixed global class distribution (GLI-TTA-F). *I.F.* is the Imbalanced Factor of Global Class-Imbalance.

Time		$t \rightarrow$															Inst.Avg.	Cat.Avg.
I.F.	Method	motion	snow	fog	shot	defocus	contrast	zoom	brightness	frost	elastic	glass	gaussian	pixelate	jpeg	impulse		
10	TEST	34.33	24.66	24.44	63.42	40.23	41.82	39.59	10.09	37.61	24.12	51.18	81.32	56.22	30.63	69.61	41.95	43.65
	BN (Nado et al. 2020)	66.45	71.35	69.56	72.82	68.41	67.19	70.89	64.10	69.05	74.80	76.52	72.48	73.16	75.86	77.82	71.36	67.70
	PL (Lee et al. 2013)	66.75	72.60	72.48	73.46	71.99	69.47	72.92	72.38	74.93	79.29	80.51	75.20	74.34	81.83	83.03	74.74	72.12
	TENT (Wang et al. 2021)	66.48	73.29	71.89	76.59	72.62	72.65	76.59	72.58	82.81	82.39	86.66	79.75	80.39	78.18	92.51	77.69	74.23
	LAME (Boudiaf et al. 2022)	27.86	18.66	18.95	63.76	35.58	38.86	34.72	5.93	33.03	17.07	47.33	82.13	55.24	23.51	67.63	38.02	40.15
	NOTE (Gong et al. 2022)	17.38	22.97	17.34	37.76	24.83	9.21	23.02	13.47	25.59	32.47	48.95	40.25	44.78	39.01	45.74	29.52	29.23
	TTAC (Su, Xu, and Jia 2022)	18.93	25.76	16.80	62.41	29.31	17.90	17.12	11.83	23.16	21.18	43.19	42.41	58.57	31.61	63.61	32.25	32.12
	RoTTA (Yuan, Xie, and Li 2023)	14.79	27.50	16.23	37.10	31.86	15.50	16.38	12.49	23.16	32.05	43.41	32.84	33.77	30.66	46.35	27.61	26.35
TRIBE		12.78	20.20	13.10	25.32	19.64	12.98	13.57	9.04	16.01	20.76	33.25	22.58	31.51	26.13	36.88	20.92 _(+6.69)	22.40 _(+3.92)
100	TEST	32.32	23.57	24.50	64.49	34.02	37.75	40.11	9.52	32.04	23.20	47.05	85.84	58.88	31.64	66.38	40.74	43.83
	BN (Nado et al. 2020)	67.35	70.54	69.49	70.58	66.42	66.95	71.03	61.86	64.97	71.87	75.46	71.87	74.17	74.86	77.80	70.35	53.07
	PL (Lee et al. 2013)	67.51	70.42	70.22	72.52	65.70	69.45	71.99	63.24	69.33	71.55	82.85	78.53	82.16	72.48	87.49	73.03	57.53
	TENT (Wang et al. 2021)	68.28	70.90	70.98	71.19	67.96	68.60	70.34	66.06	74.29	72.96	81.48	80.23	73.61	68.40	89.59	72.99	58.65
	LAME (Boudiaf et al. 2022)	25.67	16.91	19.01	65.21	29.18	34.38	35.59	5.33	26.84	16.18	41.97	86.84	57.71	24.33	62.55	36.51	42.16
	NOTE (Gong et al. 2022)	19.25	23.65	17.76	41.36	26.19	7.99	27.48	13.12	25.30	24.90	46.81	39.95	48.47	41.85	46.17	30.02	29.88
	TTAC (Su, Xu, and Jia 2022)	15.09	36.76	17.92	75.54	42.37	18.72	18.81	14.08	29.62	18.64	42.49	52.78	60.41	33.94	75.38	36.84	37.13
	RoTTA (Yuan, Xie, and Li 2023)	17.23	34.06	18.36	46.13	50.44	13.64	19.17	12.67	24.41	34.50	45.96	38.98	41.44	34.71	50.65	32.16	29.32
TRIBE		13.03	23.49	11.46	29.26	25.06	13.52	13.60	7.75	14.53	21.55	32.20	28.45	42.21	24.70	35.84	22.44 _(+7.58)	25.50 _(+3.82)
200	TEST	31.64	23.19	24.93	64.70	32.48	36.10	40.71	9.70	30.88	22.83	45.89	86.68	60.77	32.13	65.28	40.53	43.77
	BN (Nado et al. 2020)	67.52	71.13	68.28	72.43	69.53	67.61	71.27	64.79	66.18	72.30	75.16	72.21	73.15	73.73	77.93	70.88	50.67
	PL (Lee et al. 2013)	66.93	71.05	68.36	72.12	68.41	67.11	70.15	66.09	69.44	76.05	74.31	81.23	79.00	82.89	74.26	72.49	54.20
	TENT (Wang et al. 2021)	67.47	70.11	68.45	72.12	68.14	69.75	72.25	68.23	70.96	82.62	78.24	80.29	69.62	76.01	87.53	73.45	54.96
	LAME (Boudiaf et al. 2022)	24.53	16.35	19.53	66.26	27.57	32.22	36.33	5.67	26.01	16.09	40.66	87.27	59.47	25.16	60.46	36.24	42.16
	NOTE (Gong et al. 2022)	20.02	21.98	18.90	38.96	26.09	10.68	28.46	12.24	25.11	23.82	49.06	37.27	45.89	37.71	49.46	29.71	30.28
	TTAC (Su, Xu, and Jia 2022)	14.79	37.62	18.28	73.19	43.39	17.16	21.72	14.83	32.26	17.29	41.73	63.49	61.48	34.94	77.21	37.96	38.07
	RoTTA (Yuan, Xie, and Li 2023)	17.65	36.33	18.05	47.50	54.24	12.06	23.06	13.00	24.71	33.07	46.78	40.08	45.04	34.63	53.89	33.34	31.35
TRIBE		13.09	24.98	11.75	30.07	31.05	11.44	12.24	8.89	14.57	21.54	30.74	29.22	44.68	24.53	37.62	23.10 _(+6.61)	27.03 _(+3.25)

Table 19: Average classification error on CIFAR10-C while continually adapting to different corruptions at the highest severity 5 with globally and locally class-imbalanced test stream and varying global class distribution (GLI-TTA-V). *I.F.* is the Imbalanced Factor of Global Class-Imbalance.

Time		$t \rightarrow$															Inst.Avg.	Cat.Avg.
I.F.	Method	motion	snow	fog	shot	defocus	contrast	zoom	brightness	frost	elastic	glass	gaussian	pixelate	jpeg	impulse		
10	TEST	28.77	39.86	49.79	69.09	27.63	54.59	27.99	29.54	44.07	37.23	53.74	70.67	75.05	40.02	39.68	45.85	46.65
	BN (Nado et al. 2020)	38.16	45.10	49.92	48.81	38.11	40.94	38.24	38.78	43.47	47.86	50.36	51.42	43.32	49.43	52.61	45.10	42.47
	PL (Lee et al. 2013)	37.72	45.05	51.70	52.17	49.07	58.69	57.28	62.25	71.39	80.31	89.22	90.71	90.82	91.31	94.69	68.16	66.62
	TENT (Wang et al. 2021)	37.49	46.08	49.90	58.95	61.56	77.53	79.31	83.31	89.53	92.41	95.54	94.25	96.23	97.39	97.14	77.11	76.51
	LAME (Boudiaf et al. 2022)	24.41	35.55	46.44	69.22	23.43	53.74	24.10	24.95	40.87	31.09	50.85	70.49	76.78	34.96	35.37	42.82	45.35
	NOTE (Gong et al. 2022)	46.39	51.68	58.85	60.81	49.10	44.32	46.65	50.77	55.80	59.31	66.49	68.58	62.77	68.34	81.11	58.07	58.46
	TTAC (Su, Xu, and Jia 2022)	27.40	40.97	42.80	52.53	31.06	43.14	30.37	27.22	35.99	37.00	41.36	46.39	48.48	39.78	33.90	38.56	38.68
	RoTTA (Yuan, Xie, and Li 2023)	33.49	42.91	46.70	48.84	34.29	42.39	35.96	27.79	37.72	39.76	42.11	42.03	37.77	38.54	43.06	39.56	39.77
TRIBE		26.57	33.88	38.47	37.85	29.18	29.95	26.37	24.56	30.29	34.70	39.22	39.86	34.31	37.18	40.38	33.52 _(+5.04)	34.49 _(+4.19)
100	TEST	26.75	39.04	49.74	68.37	26.61	54.67	28.02	28.30	43.17	37.31	53.97	67.81	76.96	38.39	40.97	45.34	46.94
	BN (Nado et al. 2020)	37.59	45.00	51.81	46.97	38.39	41.58	38.85	35.85	43.22	47.40	52.84	49.88	43.64	49.74	54.48	45.15	38.80
	PL (Lee et al. 2013)	35.52	44.11	48.76	47.82	42.23	46.55	47.02	45.75	51.01	57.06	61.47	60.44	60.39	69.03	74.24	52.83	48.39
	TENT (Wang et al. 2021)	34.44	44.30	49.41	48.43	49.74	58.09	55.75	60.86	69.78	77.24	81.14	81.65	86.06	91.37	93.01	65.42	63.48
	LAME (Boudiaf et al. 2022)	22.62	34.30	46.18	69.26	21.68	53.59	24.73	23.37	40.83	31.58	51.10	67.53	79.26	34.07	36.98	42.47	47.82
	NOTE (Gong et al. 2022)	45.52	49.55	56.41	46.55	43.69	45.97	44.96	47.25	51.43	57.02	64.62	67.06	61.33	60.21	73.02	55.16	55.95
	TTAC (Su, Xu, and Jia 2022)	27.83	48.10	46.13	55.94	26.89	46.97	29.61	26.84	38.90	39.00	43.78	48.33	61.80	49.60	41.30	42.07	41.05
	RoTTA (Yuan, Xie, and Li 2023)	30.41	41.67	48.80	49.32	37.21	38.85	42.56	25.06	43.50	50.26	44.77	46.27	48.90	39.18	46.22	42.20	39.93
TRIBE		24.78	32.94	38.48	36.37	30.46	30.78	28.77	22.15	30.92	36.65	41.44	39.00	37.35	35.85	40.50	33.76 _(+8.31)	34.63 _(+4.17)
200	TEST	25.83	39.37	49.41	68.26	26.85	54.35	27.87	28.14	43.23	37.65	53.81	66.43	77.71	37.59	40.92	45.16	40.61
	BN (Nado et al. 2020)	36.68	46.62	51.81	46.94	41.78	40.76	39.42	35.77	42.80	47.26	52.04	51.40	43.72	49.73	54.46	45.37	33.45
	PL (Lee et al. 2013)	35.28	43.45	49.46	45.54	44.90												

Time	$t \rightarrow$															Avg.
Method	motion	snow	fog	shot	defocus	contrast	zoom	brightness	frost	elastic	glass	gaussian	pixelate	jpeg	impulse	
TEST	34.8	25.1	26.0	65.7	46.9	46.7	42.0	9.3	41.3	26.6	54.3	72.3	58.5	30.3	72.9	43.5
BN (Nado et al. 2020)	73.2	73.4	72.7	77.2	73.7	72.5	72.9	71.0	74.1	77.7	80.0	76.9	75.5	78.3	79.0	75.2
PL (Lee et al. 2013)	73.9	75.0	75.6	81.0	79.9	80.6	82.0	83.2	85.3	87.3	88.3	87.5	87.5	87.5	88.2	82.9
TENT (Wang et al. 2021)	74.3	77.4	80.1	86.2	86.7	87.3	87.9	87.4	88.2	89.0	89.2	89.0	88.3	89.7	89.2	86.0
LAME (Boudiaf et al. 2022)	29.5	19.0	20.3	65.3	42.4	43.4	36.8	5.4	37.2	18.6	51.2	73.2	57.0	22.6	71.3	39.5
CoTTA (Wang et al. 2022b)	77.1	80.6	83.1	84.4	83.9	84.2	83.1	82.6	84.4	84.2	84.5	84.6	82.7	83.8	84.9	83.2
NOTE (Gong et al. 2022)	18.0	22.1	20.6	35.6	26.9	13.6	26.5	17.3	27.2	37.0	48.3	38.8	42.6	41.9	49.7	31.1
TTAC (Su, Xu, and Jia 2022)	20.7	18.7	13.1	38.9	16.9	17.4	12.7	8.6	19.5	24.6	32.1	33.9	25.0	24.5	38.8	23.0
RoTTA (Yuan, Xie, and Li 2023)	18.1	21.3	18.8	33.6	23.6	16.5	15.1	11.2	21.9	30.7	39.6	26.8	33.7	27.8	39.5	25.2
TRIBE	14.4	13.3	9.3	20.7	12.8	10.5	10.3	6.8	13.1	18.1	24.8	20.4	18.2	21.3	28.4	16.1 _(<i><6.9</i>)

Table 21: Average classification error of the task CIFAR10 \rightarrow CIFAR10-C while continually adapting to different corruptions at the highest severity 5 with correlative sampled test stream under the PTTA setup.

Time	$t \rightarrow$															Avg.
Method	motion	snow	fog	shot	defocus	contrast	zoom	brightness	frost	elastic	glass	gaussian	pixelate	jpeg	impulse	
TEST	30.8	39.5	50.3	68.0	29.3	55.1	28.8	29.5	45.8	37.2	54.1	73.0	74.7	41.2	39.4	46.4
BN (Nado et al. 2020)	48.5	54.0	58.9	56.2	46.4	48.0	47.0	45.4	52.9	53.4	57.1	58.2	51.7	57.1	58.8	52.9
PL (Lee et al. 2013)	50.6	62.1	73.9	87.8	90.8	96.0	94.8	96.4	97.4	97.2	97.4	97.4	97.3	97.4	97.4	88.9
TENT (Wang et al. 2021)	53.3	77.6	93.0	96.5	96.7	97.5	97.1	97.5	97.3	97.2	97.1	97.7	97.6	98.0	98.3	92.8
LAME (Boudiaf et al. 2022)	22.4	30.4	43.9	66.3	21.3	51.7	20.6	21.8	39.6	28.0	48.7	72.8	74.6	33.1	32.3	40.5
CoTTA (Wang et al. 2022b)	49.2	52.7	56.8	53.0	48.7	51.7	49.4	48.7	52.5	52.2	54.3	54.9	49.6	53.4	56.2	52.2
NOTE (Gong et al. 2022)	45.7	53.0	58.2	65.6	54.2	52.0	59.8	63.5	74.8	91.8	98.1	98.3	96.8	97.0	98.2	73.8
TTAC (Su, Xu, and Jia 2022)	28.0	35.4	39.0	45.5	27.3	34.0	27.1	24.9	32.4	32.9	39.2	43.7	34.3	37.0	31.3	34.1
RoTTA (Yuan, Xie, and Li 2023)	31.8	36.7	40.9	42.1	30.0	33.6	27.9	25.4	32.3	34.0	38.8	38.7	31.3	38.0	42.9	35.0
TRIBE	28.3	32.6	37.7	38.4	28.6	28.3	26.2	25.1	31.4	34.0	38.7	39.4	32.1	38.4	39.5	33.3 _(<i><6.8</i>)

Table 22: Average classification error of the task CIFAR100 \rightarrow CIFAR100-C while continually adapting to different corruptions at the highest severity 5 with correlative sampled test stream under the PTTA setup.